



T.C.
YÜKSEKÖĞRETİM KURULU BAŞKANLIĞI
ANKARA

05.03.2024

OKUL TANIMA BELGESİ

T.C. Kimlik No : 44749306658
Adı Soyadı : İSMAİL ALTUNTAŞ
Ülke : TUNUS
Üniversite : Université de Monastir
Durumu : Kurulumuzda mevcut uluslararası listelerde yer almaktadır.

Açıklama

Yurtdışındaki yükseköğretim kurumlarından örgün eğitim yoluyla alınan diplomaların denklik işlemi, 2547 sayılı Yükseköğretim Kanunu'nun 2880 sayılı kanunla değişik 7/p maddesi ile 05.12.2017 tarihli Resmi Gazete'de yayımlanan "Yurtdışı Yükseköğretim Diplomaları Tanıma ve Denklik Yönetmeliği" hükümleri uyarınca yapılmakta olup, söz konusu Yönetmelik yatay geçiş, dikey geçiş ve lisans tamamlama gibi kavramları kapsamamaktadır.

Yurtdışındaki yükseköğretim kurumlarından uzaktan öğretim yoluyla alınacak diplomalar ise söz konusu Yönetmeliğin 10. maddesi ve ilgili mevzuat çerçevesinde değerlendirilmektedir.

Öğrenim dili Türkçe olan yurt dışındaki yükseköğretim programlarından alınan diplomalar için yapılan başvurular Yönetmelik'in 7. madde, 6. fıkra, (ç) bendi "*Türkiye'nin taraf olduğu uluslararası anlaşmalarla öğrenim dilinin Türkçe olduğu belirlenen programlar veya Yükseköğretim Kurulunca tanınan yurtdışındaki Türkçe yükseköğretim programları dışında, yükseköğretim kurumlarının açtığı ve öğrenim dili Türkçe olan programlardan alınan diplomalar için yapılan başvurular reddedilir.*" hükmü çerçevesinde karara bağlanacaktır.

Diploma denklik başvurusunda aranacak belgeler ile inceleme ve değerlendirme usul ve esasları Yurtdışı Yükseköğretim Diplomaları Tanıma ve Denklik Yönetmeliği'nde belirtilmiş olup; ilgili Yönetmelik ve detaylı bilgiye Yükseköğretim Kurulu web sayfasından ulaşılabilmektedir.

Yatay geçiş başvuruları, 08.02.2008 tarih ve 636/2732 sayılı yazımız ile "Yükseköğretim Kurumları Arasında Ön lisans ve Lisans Düzeyindeki Programlar Arasında Geçiş, Çift Anadal, Yan Dal ile Kurumlar Arası Kredi Transferi Yapılması Esaslarına İlişkin Yönetmelik" hükümlerine; lisansüstü eğitim başvuruları ise 26.09.2017 tarih ve 64528 sayılı yazı ile "Lisansüstü Eğitim ve Öğretim Yönetmeliği" hükümlerine uygun olarak, alınan dersler incelenmek suretiyle başvuru yapılan Üniversite tarafından değerlendirilmekte ve karara bağlanmaktadır.

2547 Sayılı Kanun'un 11 b/5 maddesi uyarınca yurtdışında yapılan doktora eğitimleri Üniversitelerarası Kurul tarafından değerlendirilmektedir. Yurtdışında yapılan doktora eğitiminin Türkiye'de yapılan doktora eşdeğer olup olmayacağı hususunda önceden herhangi bir görüş belirtmek mümkün olmadığı gibi, söz konusu eşdeğerlik, doktora tamamlandıktan sonra ilgili komisyon ve kurullar tarafından incelenmektedir.

Öte yandan diploma denklik başvuruları, ilgili Komisyon ve Kurullar tarafından münferiden değerlendirildiğinden yurt dışındaki yükseköğretim kurumlarından alınmış ön lisans, lisans ve yüksek lisans diplomalarının ülkemizdeki diplomalara eşdeğer olup olmayacağı hususunda önceden herhangi bir görüş belirtmek mümkün olmadığı gibi, eğitim alınan yükseköğretim kurumunun tanınırlığına ilişkin olarak Kurulumuzun yeni kararlar alma hakkı saklıdır.

Yurt dışında yükseköğrenim görmek isteyen öğrencilerin konuyla ilgili güncel gelişme ve kararları Kurulumuz internet adresinden takip etmeleri yararlarına olacaktır.

Bilgilerinizi rica ederim.

***BU BELGE DENKLİK BELGESİ YERİNE GEÇMEZ**

Bu belgenin doğruluğunu barkod numarası ile <https://www.turkiye.gov.tr/belge-dogrulama> adresinden, mobil cihazlarınıza yükleyeceğiniz e-Devlet Kapısına ait Barkodlu Belge Doğrulama veya YÖK Mobil uygulaması vasıtası ile yandaki karekod okutularak kontrol edilebilir.



MATERIALS SCIENCE IN SEMICONDUCTOR PROCESSING

Publisher name: ELSEVIER SCI LTD

Journal Impact Factor™

4.1

2022

3.7

Five Year

JCR Category	Category Rank	Category Quartile
ENGINEERING, ELECTRICAL & ELECTRONIC <i>in SCIE edition</i>	97/275	Q2
MATERIALS SCIENCE, MULTIDISCIPLINARY <i>in SCIE edition</i>	139/344	Q2
PHYSICS, APPLIED <i>in SCIE edition</i>	45/160	Q2
PHYSICS, CONDENSED MATTER <i>in SCIE edition</i>	21/67	Q2

Source: Journal Citation Reports 2022. [Learn more](#)

Journal Citation Indicator™

0.91

2022

0.92

2021

JCI Category	Category Rank	Category Quartile
ENGINEERING, ELECTRICAL & ELECTRONIC <i>in SCIE edition</i>	106/352	Q2
MATERIALS SCIENCE, MULTIDISCIPLINARY <i>in SCIE edition</i>	118/424	Q2
PHYSICS, APPLIED <i>in SCIE edition</i>	42/178	Q1
PHYSICS, CONDENSED MATTER <i>in SCIE edition</i>	16/76	Q1

The Journal Citation Indicator is a measure of the average Category Normalized Citation Impact (CNCI) of citable items (articles and reviews) published by a journal over a recent three year period. It is used to help you evaluate journals based on other metrics besides the Journal Impact Factor (JIF). [Learn more](#)



Full text at publisher



Export

Add To Marked List

Experimental insights toward carrier localization in in-rich InGaAs/InP as candidate for SWIR detection: Microstructural analysis combined with optical investigation

By Ben Arbia, M (Ben Arbia, Marwa) [1]; Demir, I (Demir, Ilkay) [2]; Kaur, N (Kaur, Navpreet) [3]; Saidi, F (Saidi, Faouzi) [1], [4]; Zappa, D (Zappa, Dario) [3]; Comini, E (Comini, Elisabetta) [3]; Altuntas, I (Altuntas, Ismail) [2]; Maaref, H (Maaref, Hassen) [1]

[View Web of Science ResearcherID and ORCID](#) (provided by Clarivate)

Source MATERIALS SCIENCE IN SEMICONDUCTOR PROCESSING

Volume: 153
DOI: 10.1016/j.mssp.2022.107149

Article Number 107149

Published JAN 2023

Early Access OCT 2022

Indexed 2023-03-29

Document Type Article

Abstract
Hyperspectral imaging has been flourished thanks to the huge investigation of the infrared spectrum from NIR to LWIR bands. The ternary InGaAs has been investigated herein in the context of studying the structural de-pendences of localization phenomenon by X-ray diffraction (XRD), scanning electron microscopy-energy dispersive X-ray (SEM-EDX), Raman, ultraviolet-visible (UV-vis), and photoluminescence (PL) techniques. Using metal-organic vapor phase epitaxy (MOVPE), we succeed to grow the InGaAs directly on InP substrate at 560 degrees C as an active layer with indium concentration exceeding the "golden" value (53%) to enlarge its cutoff absorption wavelength. X-ray diffraction proved a good crystallinity of the heterostructure with a sharp peak related to the thick substrate and another peak attributed to the thin layer of InGaAs. Moreover, an interfacial layer appeared at the logarithmic scale of XRD patterns and was confirmed by Raman analysis. The SEM-EDX revealed an average indium concentration (62%), almost the growth concentration. However, a cross-section compositional profile over the heterostructure showed an inhomogeneous distribution of the indium. This is predictable from the composition fluctuation in the indium-containing alloys and the volatility (surface segregation) of As (In). On the other side, the optical investigation of InGaAs demonstrated an anomalous behavior of luminescence versus temperature, manifested by the S-shape feature. This trend stems from the potential fluctuation induced by the non-uniform distribution of indium. A numerical simulation was developed based on the localized state ensemble (LSE) model to well-reproduce this anomaly by giving the best fitting parameters and comparing them with those calculated using the semi-empirical models (V_{in} similar to a and P_a center dot ssler). The results reported here will help in optimizing the epitaxy design of future InGaAs/InP and further studying its surface morphology and device performance.

Keywords
Author Keywords: InGaAs; InP; X-ray diffraction; SEM-EDX; Raman; Temperature dependent photoluminescence; (TDPL); Carrier localization

Keywords Plus: MOLECULAR-BEAM EPITAXY; QUANTUM-WELLS; TEMPERATURE-DEPENDENCE; INTERFACE ABRUPTNESS; RAMAN-SPECTROSCOPY; GROWTH; PHOTOLUMINESCENCE; SUPERLATTICES; HETEROSTRUCTURE; LUMINESCENCE

Citation Network

In Web of Science Core C

0 Citations

[Create citation alert](#)

73 Cited References

[View Related Records](#)

You may also like...

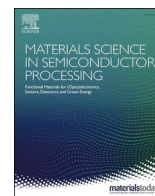
Lim, ACH; Gupta, R; Hill, Determination of InAsP band offsets using blue asymmetric multiple quantum wells PHYSICS OF SEMICONDUCTORS

GUSTAFSSON, A; NILSSON, LAYER TO LAYER QUANTUM FLUCTUATIONS IN A GALLIUM QUANTUM-WELL STRUCTURE CATHODOLUMINESCENCE INSTITUTE OF PHYSICS

Akahane, K; Yamamoto, al. Control of wavelength and photoluminescence for grown on InP(311)B using embedding method PHYSICA STATUS SOLIDI STATE PHYSICS

TABATA, A; BENYATTOU, al. PHOTOLUMINESCENCE OF STRAINED INGAAS/INP HETEROSTRUCTURES APPLIED SURFACE SCIENCE

Yuan, XW; Wang, Q; Zhang



Experimental insights toward carrier localization in in-rich InGaAs/InP as candidate for SWIR detection: Microstructural analysis combined with optical investigation

Marwa Ben Arbia^{a,*}, Ilkay Demir^b, Navpreet Kaur^c, Faouzi Saidi^{a,d}, Dario Zappa^c, Elisabetta Comini^c, Ismail Altuntaş^b, Hassen Maaref^a

^a Laboratoire de Micro-optoélectronique et Nanostructures (LR99ES29), Université de Monastir, Faculté des Sciences Monastir, Avenue de l'Environnement, 5019, Monastir, Tunisia

^b Department of Nanotechnology Engineering, Nanophotonics Research and Application Center Sivas Cumhuriyet University, Sivas, 58140, Turkey

^c SENSOR Laboratory, Department of Information Engineering (DII), University of Brescia, Via D. Valotti 9, 25133, Brescia, Italy

^d Institut Supérieur des Sciences Appliqués et Technologie de Sousse, Université de Sousse, Tunisia

ARTICLE INFO

Keywords:

InGaAs/InP
X-ray diffraction
SEM-EDX
Raman
Temperature dependent photoluminescence (TDPL)
Carrier localization

ABSTRACT

Hyperspectral imaging has been flourished thanks to the huge investigation of the infrared spectrum from NIR to LWIR bands. The ternary InGaAs has been investigated herein in the context of studying the structural dependences of localization phenomenon by X-ray diffraction (XRD), scanning electron microscopy-energy dispersive X-ray (SEM-EDX), Raman, ultraviolet–visible (UV–vis), and photoluminescence (PL) techniques. Using metal-organic vapor phase epitaxy (MOVPE), we succeeded to grow the InGaAs directly on InP substrate at 560 °C as an active layer with indium concentration exceeding the “golden” value (53%) to enlarge its cutoff absorption wavelength. X-ray diffraction proved a good crystallinity of the heterostructure with a sharp peak related to the thick substrate and another peak attributed to the thin layer of InGaAs. Moreover, an interfacial layer appeared at the logarithmic scale of XRD patterns and was confirmed by Raman analysis. The SEM-EDX revealed an average indium concentration (62%), almost the growth concentration. However, a cross-section compositional profile over the heterostructure showed an inhomogeneous distribution of the indium. This is predictable from the composition fluctuation in the indium-containing alloys and the volatility (surface segregation) of As (In). On the other side, the optical investigation of InGaAs demonstrated an anomalous behavior of luminescence versus temperature, manifested by the S-shape feature. This trend stems from the potential fluctuation induced by the non-uniform distribution of indium. A numerical simulation was developed based on the localized state ensemble (LSE) model to well-reproduce this anomaly by giving the best fitting parameters and comparing them with those calculated using the semi-empirical models (Viña and Pässler). The results reported here will help in optimizing the epitaxy design of future InGaAs/InP and further studying its surface morphology and device performance.

1. Introduction

Since its discovery by W. Herschel, infrared spectrum has been increasingly investigated in a multitude of fields: optoelectronic, medicine, agriculture, military, spectroscopy, and planetary space missions. This multi-spectral radiation is divided into four sub-bands: near infrared NIR (0.75–1 μm), short wave infrared SWIR (1–2.5 μm), medium wave infrared MWIR (3–5 μm), and long wave infrared LWIR (8–12 μm), corresponding to the atmosphere transmission windows.

Compared to their counterparts, SWIR is considered the eye-safety band, englobing the benefits of visible and MWIR spectral bands: it is more penetrative and has better transmission over the atmosphere ($\lambda > \lambda_{VIS}$) and better spatial resolution ($\lambda < \lambda_{MWIR}$) [1]. Due to its unique properties and its multi-functional applications, SWIR has been of great interest to evolve image detection, remote control, food inspection, surveillance in airports, etc ... [2] One of the most suitable material operating at SWIR range is the ternary indium gallium arsenide (InGaAs) that serves as a key driver of SWIR detection technology due to its small bandgap,

* Corresponding author.

E-mail address: benarbiamarwa94@gmail.com (M. Ben Arbia).

<https://doi.org/10.1016/j.mssp.2022.107149>

Received 20 April 2022; Received in revised form 13 September 2022; Accepted 2 October 2022

Available online 9 October 2022

1369-8001/© 2022 Published by Elsevier Ltd.

adjustable by indium composition change, and its operation without cooling system compared with its counterpart, the mercury cadmium telluride (MCT) and the free/doped selenium lead sulfide (PbS(Se)) material [3–5]. Its cut-off wavelength around 1.7 μm , obtained for the “golden” indium concentration ($x_{\text{In}} = 0.53$), promotes the use of InGaAs for telecommunication applications. Tada et al. have investigated the heterostructure InGaAs/InP as a single-photon diode operating at 1.55 μm in a sinusoidal regime reaching a detection efficiency of approximately 60% with a low probability of dark counts per gate (4.7×10^{-4}) [6]. The elaboration of such structures was commonly conducted utilizing molecular beam epitaxy (MBE) or metal-organic vapor phase epitaxy (MOVPE). Jiao et al. have grown 1 μm -InGaAs on (100) oriented InP substrate in Riber C21T MBE system devoted to photocathode processing, with 150 nm-InP buffer layer and 500 nm-InP cap layers at 500 $^{\circ}\text{C}$, showing a good crystallinity and a smooth surface with root mean square roughness $\text{RMS} = 0.1$ nm by using X-ray diffraction (XRD) and atomic force microscopy (AFM), expected from the lattice matching concentration of indium ($x_{\text{In}} = 0.53$) [7]. Gutowski et al. have also prepared by MBE method smooth surfaces of InGaAs at the same concentration using InAlAs buffer layer where the RMS roughness fluctuates between 0.118 and 0.127 nm at temperatures between 510 $^{\circ}\text{C}$ and 530 $^{\circ}\text{C}$ and V/III ratio going from 5 to 20 [8].

However, there are serious technical limitations related to MBE: i) the V-element sources cannot be reloaded when processing phosphorus-containing materials [9] and ii) the inherent problem in growing thick layer of indium phosphide (substrate) [8] that renders it not the most suitable for the preparation and commercialization of the InGaAs/InP heterostructures. The MOVPE system can be a good alternative due to the low pressure used for epitaxy and the low-cost production. Jiang et al. have studied the V/III ratio effect on the InGaAs/InP structures grown by MOVPE at 550 $^{\circ}\text{C}$. They have noted that increasing the V/III ratio from 64 to 256 varied the lattice mismatch between InGaAs and InP layers from 0.149% to -0.057% and the carrier concentration from $5.8 \times 10^{18} \text{ cm}^{-3}$ to $3 \times 10^{18} \text{ cm}^{-3}$ [10]. Operating at extended wavelength can be achieved for InGaAs only when ensuring high concentrations in Indium so as its strain to the InP substrate will be 3.2% for $x_{\text{In}} = 1$ [11]. However, the high Indium contents boost the defects and dislocations' generation into the structure. To engineer the strain and outweigh the propagation of dislocations, the researchers used strained superlattices, linear graded layers and compositionally-step graded buffer layers. As well, the ternary InAlAs has been frequently introduced as buffer layer in such a structure to compensate for the strain mismatch with the InGaAs layer by the calibration of indium and the reduced growth rate (0.79 $\mu\text{m}/\text{h}$) that should not be too low in order to avoid the degradation of optical quality [8]. Nevertheless, InAlAs buffer layer can lead to phase decomposition and rougher surface. Another material has been introduced as buffer layer: InAsP ternary. This latter can be a good alternative to relax the strained monolayers on the InP substrate instead of InAlAs by showing step-graded aspect [11,12] where the roughness is 7.3 nm for InAlAs Vs. 2.2 nm for InAsP. The step-graded buffer layer demonstrated by InAsP can be useful to migrate the strain mismatch for In-rich InGaAs. Li et al. have grown InGaAs at $x_{\text{In}} = 0.76$ on InP substrate with compositionally undulating step graded buffer structure with an unequal layer thickness of InAsP (2.09 μm of thickness). The same InGaAs ternary was also grown on InP by insertion of common step graded buffer structures of InAsP (2.96 μm of thickness), intentionally. The structures assured the extended wavelength of 2.3 μm compared to 2 μm for $x_{\text{In}} = 0.69$ which is worthy for SWIR application [12]. One can see the successful strategy of graded buffer layer to mitigate the imperfections of the grown heterostructure for high indium contents operating at SWIR band. Nevertheless, this technique inquires more sophisticated processes, higher costs, and much control of the growth parameters and it can also degrade the optical quality as reported in Ref. [13]. Guo et al. have reported on the interface engineering in InGaAs/InP by studying the effect of buffer layer on its emission properties: the better performance can be attended when sacrificing the

buffer layer. In 2019, Zhao et al. have experimentally investigated the surface-interface free buffered heterostructures of InGaAs/InP for different In contents and they have concluded that growing such heterostructure out of lattice matching condition will be more beneficial for higher indium concentrations (>0.53 : positive lattice mismatch system) to reduce the dislocation density and prevent the threading dislocations in the substrate from moving to the epitaxial film [14].

In this context, we suggest elaborating $\text{In}_{0.65}\text{Ga}_{0.35}\text{As}/\text{InP}$ without buffer structures to simplify the epitaxy design, to reduce the production costs as much as possible, to avoid the deterioration of optical performance, and to maintain a good surface morphology, which present our challenge in this work. The sample was subjected to structural characterization using X-Ray diffractometer (XRD), scanning electron microscopy-energy dispersive X-ray technique (SEM-EDX), Raman spectroscopy, and atomic force microscopy (AFM) to study the composition, the microstructure, the surface quality and the strain effects. The optical investigation is also conducted to study the InGaAs luminescence evolution where a numerical simulation using the localized state ensemble model is performed for comparative analysis between experimental results and semi-empirical models. All these experiments are devoted to probing the In-rich InGaAs structural properties and studying its optical behavior and their effects on the promotion of this sample for SWIR detection.

2. Experimental details

InGaAs epilayer was grown on a commercially available indium phosphide (InP) substrate which is (100) oriented, semi-insulating (SI), double side polished, and Wafer-Tech brand, by using horizontal flow reactor MOVPE system which is brand AIXTRON $1 \times 2''$ or $1 \times 3''$ 200/4 RF-S. The real time information about the growth such as reflection intensity, growth rate and temperature of substrate was obtained by Luxtron 880 nm reflectometer and light pipe assembly. InGaAs epilayer was grown thickness of 190 nm at 560 $^{\circ}\text{C}$ with the growth rate of 3 $\text{\AA}/\text{s}$. The opto-grade Trimethylgallium (TMGa, $\text{Ga}(\text{CH}_3)_3$), Trimethylindium (TMIn, $\text{In}(\text{CH}_3)_3$), and Arsine (AsH_3) sources were employed to elaborate the III-V compounds as precursors of gallium, indium, and arsenic in MOVPE set-up, transferred by using ultra-high purified N_2 and H_2 carrier gases. TMGa, TMIn and AsH_3 flows were used as 0.85, 37, and 40 sccm, respectively and V/III ratio was 136. Reactor pressure, total carrier flow and substrate rotation speed were fixed as 50 mbar, 6000 sccm, and 80 rpm, respectively. The InGaAs thin film was deposited on the InP substrate without buffer layers, which represents the challenge of this work.

The structural properties of the investigated sample were studied using X-ray diffractometer (Empyrean, PANalytical, Almelo, The Netherlands) in the Bragg-Brentano configuration with $\lambda_{\text{Cu}} = 1.54 \text{ \AA}$ anode operated at 40 kV- 40 mA and 2 θ -scanning in the range 40 $^{\circ}$ –80 $^{\circ}$.

Additionally, the microstructural analysis of the III-V alloy was performed using scanning electron microscopy (LEO 1525 model, Carl Zeiss AG, Oberkochen, Germany) operated at 10–15 kV, combined with energy dispersive X-ray spectroscopy. Raman spectra were measured by using a XploRA Nano system (Horiba Jobin Yvon Srl, Italy) formed by a confocal microscope (Olympus BX) and a 1200 gr/mm reticule. A Peltier-cooled Open Electrode CCD was used to record the Raman spectra excited by a 638 nm solid-state laser. Spectra were recorded in the Raman shift range 50–540 cm^{-1} measured at room temperature. UV-vis spectrometer (UV-2600, Shimadzu, Kyoto, Japan) was used to determine the absorption coefficient and estimate the bandgap energy of our sample at room temperature. Regarding the systematic optical investigation, we conducted temperature dependent photoluminescence TDPL measurements in the range 10 K–300 K using ionized Argon laser with $\lambda_{\text{Ar}^+} = 514.5$ nm chopped at 27 Hz, JOBIN YVIN iHRD320 1/3 m monochromatic system, and InGaAs photodetector, all connected to a lock-in amplifier system.

3. Results and discussions

3.1. Composition and microstructure

The XRD patterns around the symmetric (0 0 4) reflection shown in Fig. 1, indicates two doublet peaks (splitting into $K\alpha_1$ and $K\alpha_2$). The right-hand doublet peak is associated with the InP substrate, while the doublet peak with less intensity corresponds to the InGaAs thin film: the XRD intensity is as lower as the layer is thinner [15]. It is well to know that the peak in lower 2θ reflects the compressive strain of InGaAs to InP, which is in good agreement with the growth composition $65\% > 53\%$ (the gold concentration for lattice matched InGaAs/InP heterostructure).

To map the distribution of III- and V-elements in the investigated structure, SEM-EDX characterization was performed. The top-view SEM images at 10 KV, given in Fig. 2, Fig. 3, Fig. 4, and Fig. 5 show a pictorial representation of InGaAs surface combined with the elemental composition of four chosen areas probed by EDX spectroscopy with an average composition of 62%.

As the Indium content measured at the top surface of the heterostructure is underestimated, a cross-section microscopy was conducted to evaluate the percentage of indium within the structure, shown in Fig. 6, Fig. 7, and Fig. 8.

The atomic weight of components within the sample in the different regions (Zone 6, Zone 7, and Zone 8, as indicated in Fig. 6, Fig. 7, and Fig. 8, are displayed in Table 1.

It is clear from Table 1 that In weight is estimated by EDX about 62% therefore pretty similar to the In concentration set during the MOVPE growth (65%). Additionally, we mention the fluctuation of indium content along the probed zones which is more important as we approach the substrate. This is indicative of the non-uniform distribution of indium atoms within the structure, mostly at the surface of the specimen because of the segregation effect related to indium. Similarly, the atomic weight starts to decrease when moving far from the substrate. Notably, the Ga weight is too small compared to the N weight owing to the growth process which intervenes in such impurities through the carrier gas flow related to N_2 . Going downward the InGaAs to the substrate, the Phosphorous weight has increased from 17% (region 6) to 21% (region 7) which remained almost constant in the region 8. The presence of Phosphorus and its larger amount compared to Gallium are quite questionable in the top area. An out-diffusion of Phosphorous and/or

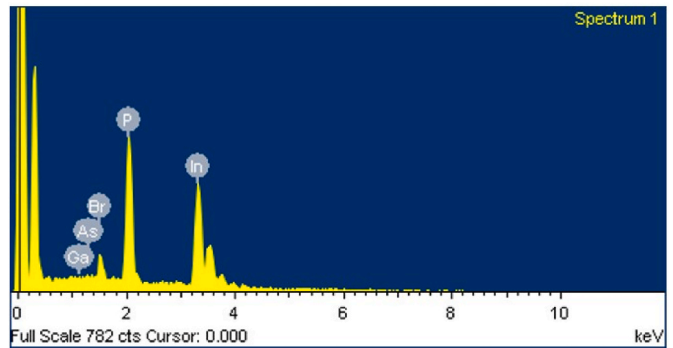
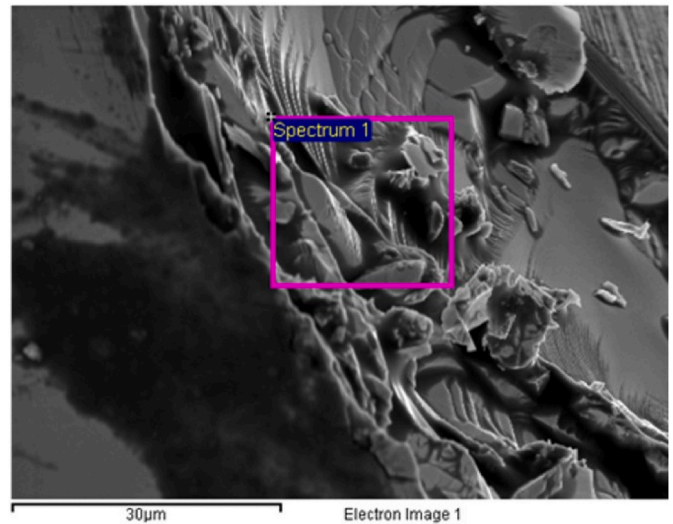


Fig. 2. Top-view micrograph taken by SEM-EDX technique in area 1 of InGaAs layer.

pipe diffusion along dislocations in defective structures could be behind this observation according to Hernandez and co-workers [16]. Moreover, the strained-layers studies have shown that tensile InGaP layer (due to the phosphorous which can induce near-surface chemical exchange between As and P atoms at the interface) or compressive InAsP layer (due to the memory effect of As-precursors in the growth chamber that allows the in-diffusion of As atoms into the substrate) can be formed for InGaAs/InP heterostructure [17–28].

Also, the high growth temperature set in our MOVPE system plays the role of catalyzer for the phosphorus out-diffusion processing [29]. To emphasize the hypothesis of non-uniform incorporation of indium within the GaAs binary, an acquisition of the compositional profile in SEM combined with EDX spectroscopy is performed to probe the atomic distribution of Indium within the investigated structure. In Fig. 9, we have done a line scan along the top area of the sample that confirms the non-uniform distribution of indium and even the phosphorous due to the inter-diffusion of Indium as mentioned earlier.

Apart from XRD and SEM-EDX techniques, Raman spectroscopy is still performant for the identification of our structure by revealing the vibration modes and the strain degree. In Fig. 10 and Table 2, we exhibited all the Raman scattering modes in InGaAs/InP sample acquired with 638 nm-excitation and interpreted in the following.

DALA or disorder-activated longitudinal acoustic phonon of InGaAs alloy is commonly located in the low-range of Raman shift ($<200\text{ cm}^{-1}$) as mentioned in Fig. 10 and Table 2. For the golden concentration of indium (0.53), the DALA vibration resides in $[100\text{--}190]\text{ cm}^{-1}$ [39]. Similarly, Sayari et al. have found the DALA band for Raman shift less than 200 cm^{-1} for the heterostructure InAlAs/InP at different Indium

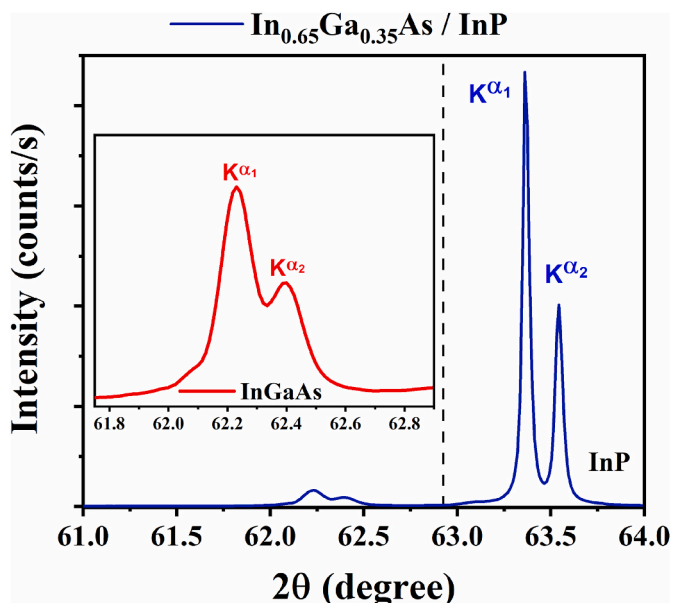


Fig. 1. XRD patterns of InGaAs/InP structure.

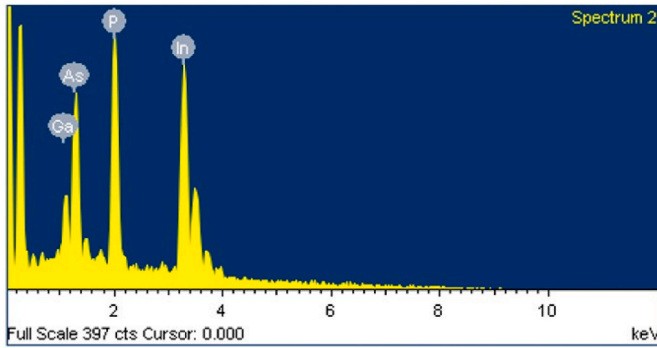
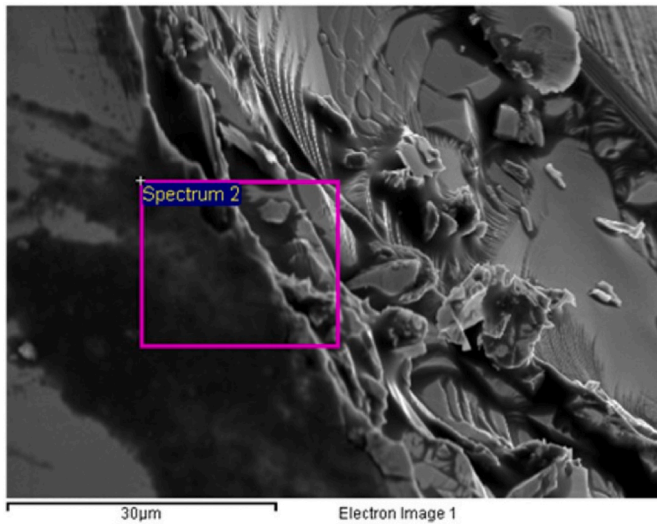


Fig. 3. Top-view micrograph taken by SEM-EDX technique in area 2 of InGaAs layer.

contents of 47.2%, 48.6%, and 53% [40].

The LO-InAs mode shows up at 214.9 cm^{-1} exhibiting the strongest peak dominating the Raman spectrum. The shoulder in the highest intensity peak of InAs vibration seems to be related to InAsP ternary (229.7 cm^{-1}). Finders et al. have recorded a shoulder near 235 cm^{-1} due to the formation of InAsP interface layer [41]. In addition, Smiri. et al. have studied the Raman scattering of InAlAs/InP at different excitation wavelengths: they have assigned the two vibrations in the range $[200\text{--}250] \text{ cm}^{-1}$ to InAs- and InAsP-like modes. Under the excitation wavelength ($\lambda_{\text{exc}} = 638 \text{ nm}$), the InAs-like mode dominates the InAsP-like one. The same trend is observed for our Raman spectrum under the same excitation $\lambda_{\text{exc}} = 638 \text{ nm}$ where the LO-InAs mode at 214.9 cm^{-1} is more intense than the LO-InAsP mode at 229.7 cm^{-1} [33]. The identification of InAsP-like mode needs to be evaluated.

As the InGaAs is an epitaxial ternary deposited onto InP without preparing buffer layers, an interfacial layer can be non-intentionally introduced to relax the strain induced by the high indium content. Probably, this layer can be either InAsP or InGaAsP. We study the nature of eventually induced layer between the InGaAs and the InP thermodynamically by calculating the standard enthalpy energies of both compounds as the following: $\Delta H_{\text{InGaAs}} = -15.13 \text{ kcal/mol}$, $\Delta H_{\text{InAsP}} = -20.35 \text{ kcal/mol}$, and $\Delta H_{\text{InGaAsP}} = -21.54 \text{ kcal/mol}$ by using Vegard law [29] and experiments ($x_{\text{In}} = 62\%$, $x_{\text{As}} = 12\%$). The InGaAs has the lowest value of enthalpy which confirms the formation of InGaAs as the main layer on InP substrate. However, comparing the enthalpies of InAsP and InGaAsP one observes that the InAsP layer can be preferentially generated at the heterointerface as it has the lowest enthalpy energy. To emphasize this interpretation, we re-investigate the XRD

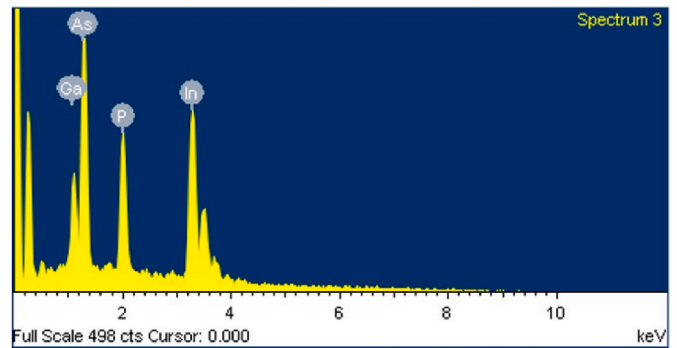
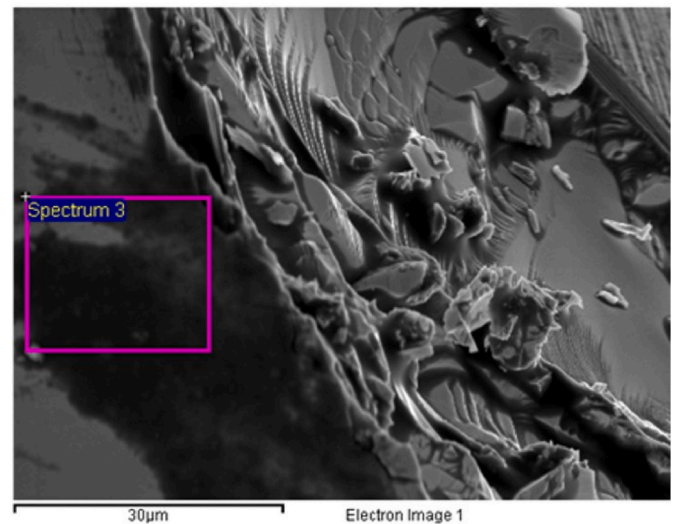


Fig. 4. Top-view micrograph taken by SEM-EDX technique in area 3 of InGaAs layer.

pattern in the semi-logarithmic scale which shows a right-hand shoulder of the InP- $K_{\alpha 1}$ (see Fig. 11) that we assigned to the interfacial layer: InAsP.

Indeed, as the enthalpies of InAsP and InGaAsP are close, the low value of InAsP formation is still an insufficient justification for the interface's nature. In that case, the type of the mismatch is decisive in the determination of the interfacial layer: the strain nature varied from compressive for InAsP/InP to tensile for InGaAsP/InP [42].

Using equation (1), the lattice parameter of the interfacial layer $a_{\text{InAsP}} = 5.8815 \text{ \AA}$ whereas the calculation by Vegard law based on SEM-EDX results gives $a_{\text{InAsP}} = 5.8833 \text{ \AA}$. This finding demonstrates that InAsP layer includes almost the same As content proved by SEM-EDX in the area (a).

$$\frac{\Delta a}{a} = \frac{-\Delta \theta_B}{\tan \theta_B} \quad (1)$$

a is the lattice parameter of the substrate, Δa is the difference in lattice parameter between the epitaxial layer and the substrate, θ_B is the Bragg diffraction angle, and $\Delta \theta_B$ is the difference in Bragg angle between the epitaxial layer and the substrate.

The diffraction peak positions located at $2\theta = 62.23^\circ$, $2\theta = 63.12^\circ$, and $2\theta = 63.36^\circ$ as displayed Fig. 11 leads to the estimate of the indium concentration $x_{\text{In}} = 73\%$ by calculating the lattice parameter $a_{\text{InGaAs}} = 5.9525 \text{ \AA}$ and the lattice mismatch: $\rho_{\text{InGaAs}} = 1.44\%$ and $\rho_{\text{InAsP}} = 0.23\%$, based on equation (1). According to the EDX-SEM measurement, the overestimate of indium content using the XRD shift is consistently related to the full relaxation of the epitaxial layer InGaAs on InP [43,44], which is exhibited in the formation of the interfacial layer (Fig. 11).

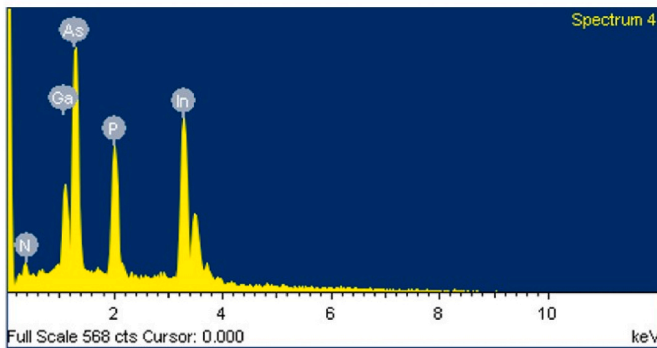


Fig. 5. Top-view micrograph taken by SEM-EDX technique in area 4 of InGaAs layer.

Meanwhile, the overestimate of As content is not reported for the InAsP ternary as the XRD pattern has almost belonged to one feature (its mismatch to InP is almost zero). Noticeably, according to Fig. 11 the interfacial layer should be thinner than the active layer due to its lower intensity. The vibration modes observed at higher wavenumbers ($> 400 \text{ cm}^{-1}$) cannot be assigned to InP modes according to reference [36]. However, 425.8 cm^{-1} and 466.7 cm^{-1} could be attributable to the local vibration mode of NN dimer on the As site (N–N_{As}) and N-isolated state [37,38], respectively. We adopt this interpretation because the SEM-EDX measurements highlight the presence of 4% of Nitrogen content within the sample that we assigned to the carrier gas used in the MOVPE set-up. We can remark that the InP modes have too low intensities compared with the Raman spectrum recorded under 532 nm in our previous work [45]. This should be related to the focus position used in experiments [46].

To get more information about the surface morphology of InGaAs, an atomic force microscopic (AFM) measurement is performed and exhibited in Fig. 12 for $5 \times 5 \mu\text{m}^2$ scan size that was reduced to $1 \times 1 \mu\text{m}^2$ in Fig. 13 for better observation of the surface topography.

As the growing surface is strongly dependent on the growth modes that shape the sample's surface, several kinds of morphology can be obtained as presented in Fig. 14.

It is worthy to notice that these different classes can be disordered and follow a non-periodic distribution as can be seen in Figs. 12 and 13. The InGaAs alloy's topography with RMS roughness of 6.9 \AA shows a complicated surface faceting with irregular planar domain and pits decorated by 2D and 3D islands as illustrated in Fig. 12 And emphasized by Fig. 13. Kitamura et al. have found the same trend and have

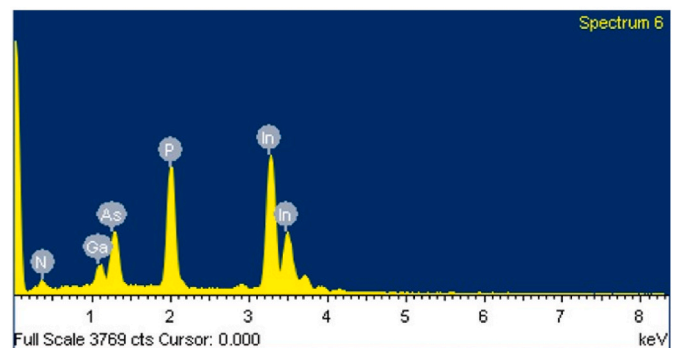
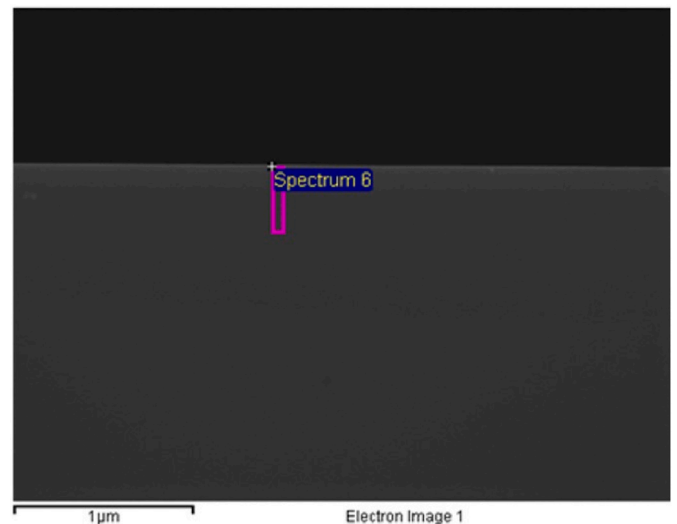


Fig. 6. Cross-section SEM micrograph over the InGaAs layer downward to the InP substrate combined with the EDX measurement in Zone 6 (spectrum 6).

associated it to the non-uniformity of In content [47]. Hence, this observation can be related to In-rich domains inducing the clusters' formation. A detailed analysis will be given in the following.

Fig. 12 (a) shows unified orientation of the stepped structure which reflects the crystallographic symmetry of the epitaxial layer [48]. The steps seem straight rather than meandered, made up of widely flat terraces and wavy edges. This straightening is supposed to be a marker of the 2D step flow growth mode [49]. However, we cannot ignore the undulation observed at the step line and the presence of cusps markedly illustrated in Fig. 12 (b, c) and Fig. 13 resulting in i) 2D pits (that can deteriorate the step structure), as indicate the white arrows in Fig. 12 (a) and the $1 \times 1 \mu\text{m}^2$ AFM image in Fig. 13 (a), and ii) 3D island, as mentioned in Figs. 12 (c) and Fig. 13 (c), that maybe assigned to clustering effect in InGaAs. Tejedor et al. [50] have evidenced the In surface segregation in InGaAs sample that results in clustering and have processed AFM measurement showing 2D to 3D transition of growth mode due to the irregular formation of clusters on the surface, similar to what we exhibited in Fig. 12 (c) and Fig. 13 (c). Gu et al. [51] have also mentioned the 2D-3D transition mode in InGaAs epitaxy due to the fact that 'In atoms can easily reach the defects on the growth surface to form some nucleation sites and form 'In-rich islands'.

Another aspect is noticed by the stepped morphology which is its irregularity that i) suggests the presence of impurities and relaxation effect due to lattice mismatched InGaAs to InP that we justify by the high indium content, set when designing the epitaxy, inducing the formation of InAsP interfacial layer demonstrated by XRD and Raman analyses, and ii) rules out the possibility that step-flow mode still governs the epitaxy of InGaAs where the observed steps could be split into smaller

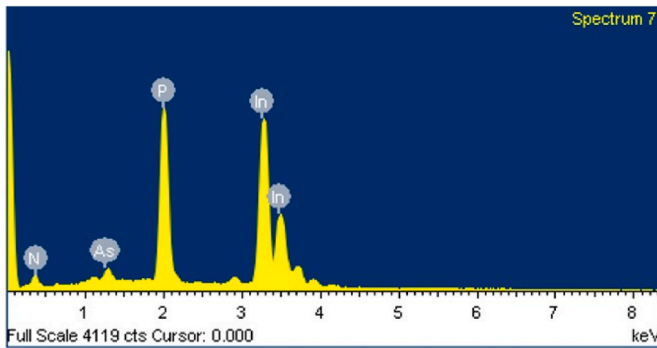
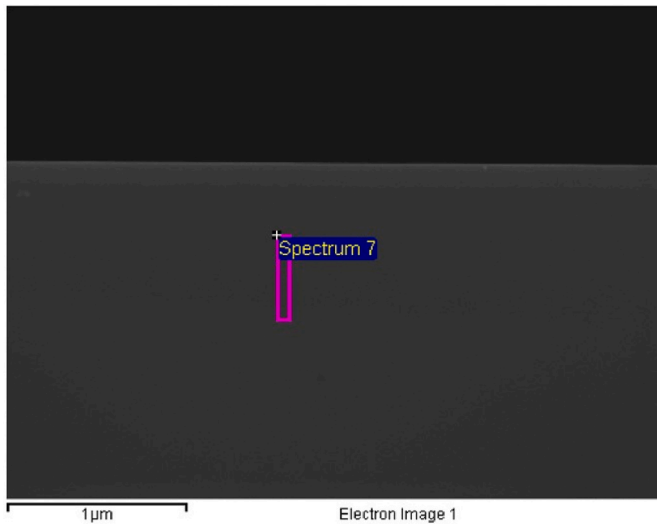


Fig. 7. Cross-section SEM micrograph over the InGaAs layer downward to the InP substrate combined with the EDX measurement in Zone 7 (spectrum 7).

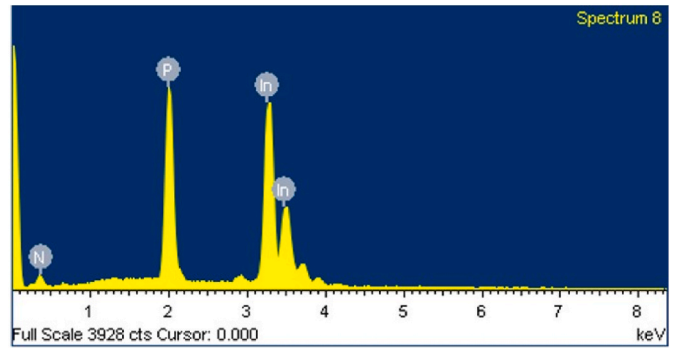
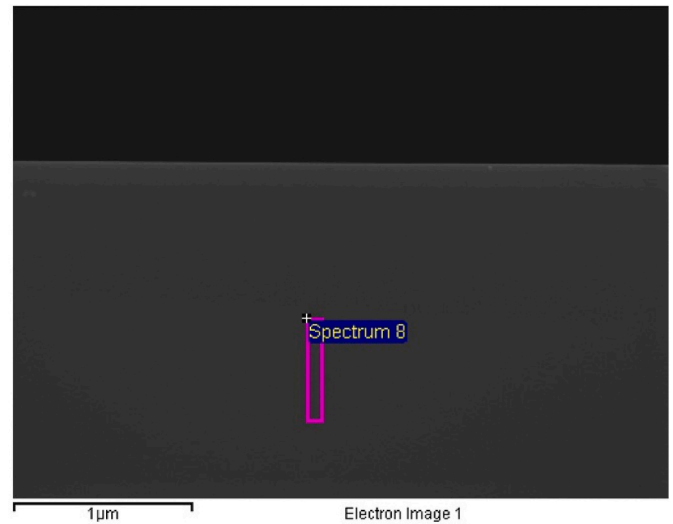


Fig. 8. Cross-section SEM micrograph over the InGaAs layer downward to the InP substrate combined with the EDX measurement in Zone 8 (spectrum 8).

ones or coalesced into larger ones giving arise to the step-bunching mode [48,52]. This growth mode could be a fingerprint of the instability of epitaxy enhanced by the relatively high growth temperature and the V/III ratio that lowers the diffusion of adatoms on the growing surface [53,54]. Jesson et al. [55] have studied the morphology instability in strained films as a cooperative mechanism of islands and pits described by their concurrent/sequential nucleation, responsible for the occurrence of 2D-3D transition. The non-periodicity and the irregularity characterizing the growing surface added to the high surface mobility of Indium compared with that of Gallium imply an inhomogeneity within the crystal. Under this condition, locally strain fluctuations occur by inducing energetic states fluctuation that directly affects the optical properties of such material. This scenario will be far discussed in the second part of the section 'optical investigation'.

Returning to the RMS roughness ($RMS = 6.9 \text{ \AA}$), a comparison is made between our value and the values found in Refs. [11,12,56] for InAlAs ($RMS = 73 \text{ \AA}$ [12]), InAsP ($RMS = 22 \text{ \AA}$ ($RMS = 36 \text{ \AA}$ optimized to 13.8 \AA by adding bottom and upper modulation layer [11]) and InAs ($RMS = 130 \text{ \AA}$ optimized to 40 \AA [56]) buffer layered InGaAs/InP, one can conclude the smooth morphology that our sample shows. This can be explained by the formation of interface layer lattice matched to InP that plays the role of unintentionally buffer layer by compensating for the dislocations and accommodating the strain in the high In content structure. This contrast is also proven by the large values of RMS (more than 40 \AA) obtained by Gu et al. [11] even when using grading profile and digital alloys in buffer layered structures. More accuracy and consistency are given to this comparison by referring to Zhao et al.'s work [42] reporting on the surface roughness of InGaAs/InP in positive and

Table 1

Atomic weight of components within the sample in the regions 6, 7, and 8.

Chemical Element	In	Ga	N	P	As
Weight (%)					
Zone 6	62	5	4	17	12
Zone 7	72	-	4	21	3
Zone 8	75	-	4	21	-

negative mismatch systems without using buffer layers: $RMS = 690 \text{ \AA}$ ($x_{In} = 0.16$), 451 \AA ($x_{In} = 0.28$), 134 \AA ($x_{In} = 0.53$), 331 \AA ($x_{In} = 0.72$), and 411 \AA ($x_{In} = 0.82$) which is exponentially higher than our sample's RMS reflecting its high surface quality that might due to the low disorder degree of crystal arrangement at the interface of positive mismatch system [14]. Such result is promoting for epitaxy design of free-buffer InGaAs/InP structure at high indium content by MOVPE system and transmission electron microscopy still highly required to examine the presence of (misfit/threading) dislocations or not in our alloying system.

3.2. Optical investigation

3.2.1. RT-UV-vis measurement

As described in Fig. 15, no sharp peak has been already observed in the RT absorption spectrum which is indicative of the high background impurities in such material [57]. Namely, we have recorded three highly absorptive spectral regions indicated by black arrows at 313 nm (3.96 eV), 475 nm (2.61 eV), and 514.5 nm (2.41 eV). We can attribute the highest one to InP material that absorbs well in the UV range [3,4] eV

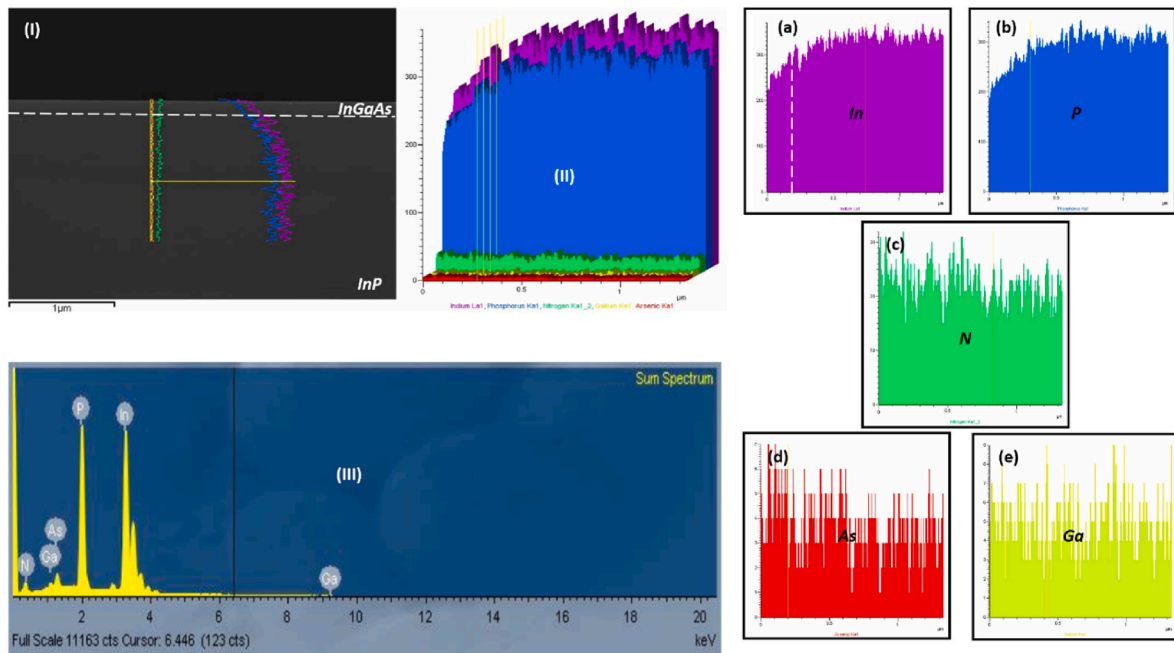


Fig. 9. Clockwise: (I) Cross-section SEM micrograph at 10 kV mapping over the InGaAs/InP heterostructure indicated by the white dashed line at 1 μm scale, (II) the composition profile in-depth of 1.3 μm of (a) Indium, (b) Phosphorous, (c) Nitrogen, (d) Arsenic, (e) Gallium, and (III) Sum EDX-spectrum of InGaAs/InP material.

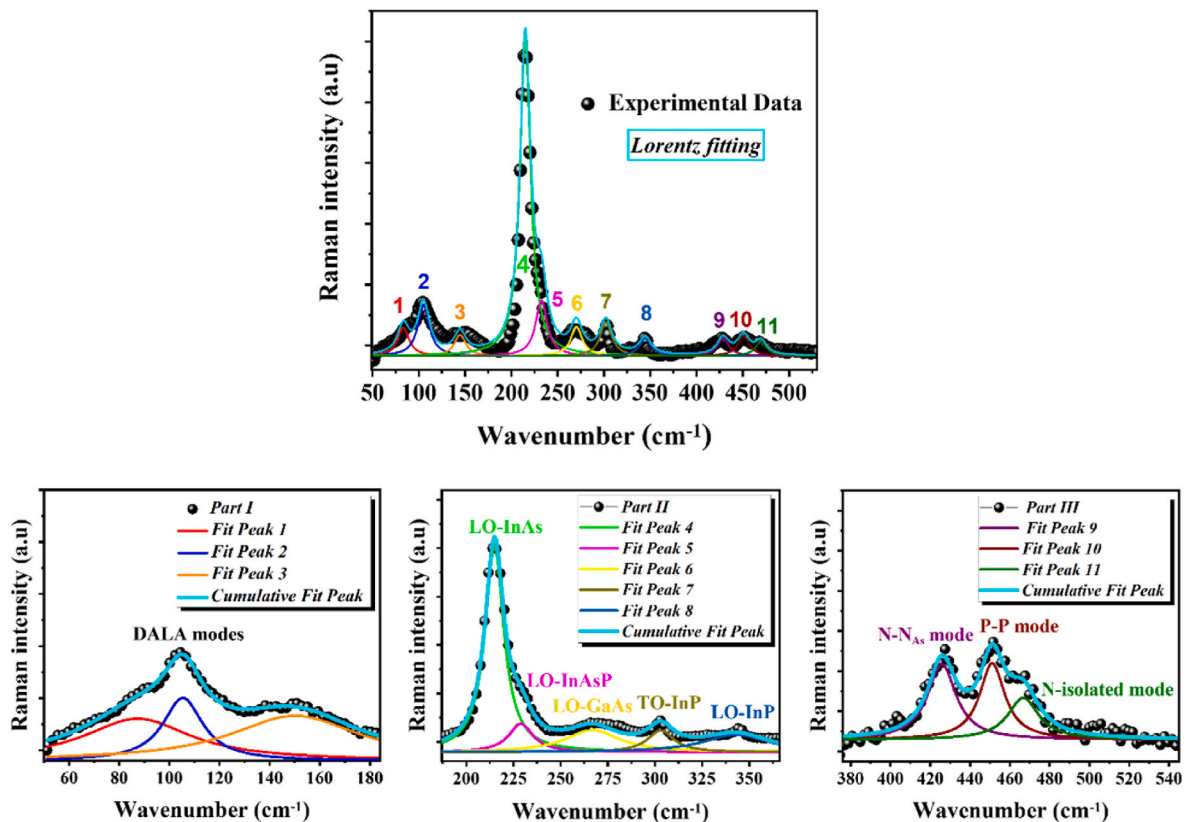


Fig. 10. Raman scattering spectra deconvoluted by Lorentzian line profiles at room temperature under 638 nm-excitation wavelength.

[58] whereas the two other peaks are assignable to the InGaAs material [13]. As mentioned above, the InP-like mode Raman intensity is lower under the 638 nm excitation than the 532 nm excitation, compared to the InAs-like mode intensity. This can be explained by the absorbance of InGaAs at these wavelengths as indicated in Fig. 15 ($\alpha^{638\text{ nm}} < \alpha^{532\text{ nm}}$):

Hernández et al. [16] reported that the probing depth of Raman scattering ϑ is inversely proportional to the absorption coefficient α ($\vartheta = \frac{1}{\alpha}$), i.e., the 532 nm wavelength will be less penetrative into the sample than that of 638 nm-wavelength where $\vartheta^{532\text{ nm}} = 137\text{ nm}$ and $\vartheta^{638\text{ nm}} = 166\text{ nm}$. The optical penetration of 638 nm-excitation wavelength

Table 2
Raman scattering modes in the InGaAs/InP structure.

Peak position (i)	Raman shift (cm ⁻¹)	$\frac{I_i}{I_4}$ ratio	FWHM (cm ⁻¹)	Raman mode	Reference
1	87.3	0.32	52.28	DALA	[30–32]
2	105.4	0.18	19.33	DALA	[30–32]
3	150.2	0.41	62.77	DALA	[30–32]
4	214.9	1	12.39	LO-InAs	[33]
5	229.7	0.16	15.19	LO-InAsP	[33,34]
6	266.1	0.39	41.21	LO-GaAs	[32,35]
7	303	0.05	7.07	TO-InP	[36]
8	343.4	0.44	63.64	LO-InP	[36]
9	425.8	0.05	17.34	N-N _{As} dimer vibration	[37]
10	451.2	0.04	15.40	P-P vibration	[16]
11	466.7	0.03	18.8	N-isolated vibration	[38]

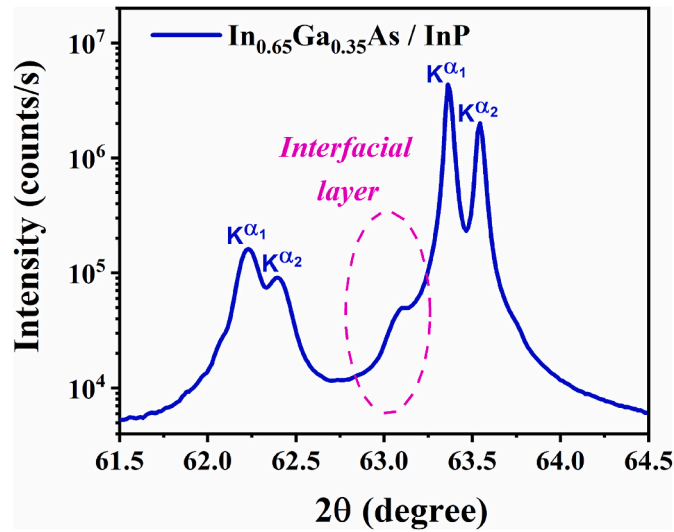


Fig. 11. XRD patterns of In_{0.65}Ga_{0.35}As/InP in semi-logarithmic scale.

within the InGaAs thin layer could explain the observation of the InAsP mode as a shoulder of the InAs vibration. By fitting the experimental data for allowed direct transition using $(\alpha h\nu)^2 = f(h\nu)$ as presented in the inset of Fig. 15, the bandgap energy of InGaAs is estimated at 0.748 eV. In the following, we have studied the temperature-dependent photoluminescence of our sample by adopting localized state ensemble simulation.

3.2.2. Temperature dependent photoluminescence in localized state ensemble (LSE) frame

The temperature dependence luminescence of semiconducting compounds has been investigated by semi-empirical models such as Varshni, Viña and Pässler models [59]. Nevertheless, abnormal emission can be detected in II-VI and III-V materials in the low temperature range. Eliseev et al. have attempted to simulate this kind of energetic evolution [60] by using equation (2):

$$E(T) = E_0 - \frac{\sigma^2}{K_B T} \quad (2)$$

E_0 is the center of the distribution function, σ is the standard deviation of the localized states' distribution and K_B is the Boltzmann constant.

As this model is reproducible only at a temperature higher than 77 K [60], another model is developed to simulate the S-shape feature: the model of "Localized State Ensemble (LSE)".

The Gaussian-type distribution of luminescence through the localized state ensemble is given by equation (3)

$$\zeta(E, T) = \omega^{DOS}(E) \cdot F(E, T) \quad (3)$$

$$F(E, T) = \frac{1}{e^{\frac{E-E_0}{K_B T}} + \frac{\tau_r}{\tau_{lr}}} \quad (4)$$

$$\omega^{DOS}(E) = \omega_0 e^{-\frac{(E-E_0)^2}{2\sigma^2}} \quad (5)$$

When we derive equation (3) with respect to the energy ($\frac{\partial \zeta}{\partial E} = 0$), the energy in the semi-empirical configuration will be given in equation (6).

$$E(T) = E_0 - A(T) \cdot K_B T \quad (6)$$

equation (2) can be expressed for an ideal semiconductor by the semi-empirical Pässler and Viña model as the following [61]:

$$E = E_B - a_B \left[1 + \frac{2}{\exp\left(\frac{\Theta_B}{T}\right) - 1} \right] - A(T) \cdot K_B T \quad (*) \quad (7)$$

$$E = E'_0 - \frac{\alpha \Theta_P}{2} \left[\sqrt{1 + \left(\frac{2T}{\Theta_P}\right)^c} - 1 \right] - A(T) \cdot K_B T \quad (**)$$

The first parameter represents the emission energy at 0 K defined by the following formula:

$$E(T=0 K) = \begin{cases} E_B - a_B = E_0 \\ E'_0 \end{cases} \quad (8)$$

The parameters derived from the second term that describes the bandgap energy shrinkage are represented herein:

α designates the derivative of energy with respect to the temperature for the limit value of high temperature such that $\alpha = -\frac{dE}{dT} \rightarrow \infty$ [62].

The temperatures Θ_P and Θ_B are estimated to be the average phonon temperature based on the Pässler and Viña approaches, respectively.

The parameter $c = \sqrt{1 + \left(\frac{\Delta E}{E}\right)^2}$ represents the phonon dispersion leading to three regimes:

$c < 2$: the regime of large dispersion

$2 < c < 3.3$: the regime of intermediate dispersion

$c > 3.3$: the regime of small dispersion

$\frac{\Delta E}{E}$ represents the phonon dispersion degree.

For higher temperatures, the bandgap energy evolution follows Eliseev's model where the parameter $A(T) = \left(\frac{\sigma}{K_B T}\right)^2$ (9)

The characteristic parameter of the thermal redistribution of carriers over localized states $A(T)$, so as $0 < A < \left(\frac{\sigma}{K_B T}\right)^2$ is estimated in the LSE configuration by solving equation (7):

$$A e^A = \left[\left(\frac{\sigma}{K_B T}\right)^2 - A \right] \left(\frac{\tau_r}{\tau_{lr}}\right) e^{\frac{E_0 - E_a}{K_B T}} \quad (10)$$

$\frac{\tau_r}{\tau_{lr}}$ represents the ratio governing the carrier localization phenomenon and ω_0 designates the amplitude of DOS distribution.

E_a is the energetic position below which carriers occupy the localized states at $T = 0$ K.

The photoluminescence investigation of In_{0.65}Ga_{0.35}As was performed at different temperatures as described in Fig. 16.

The low temperature LT PL-spectrum in Fig. 16 (a) proves the operation of the investigated sample in the SWIR range, where the inset presents the thermal evolution of the integrated PL intensity. The dependence of PL spectra on temperature is exhibited in Fig. 16 (b),

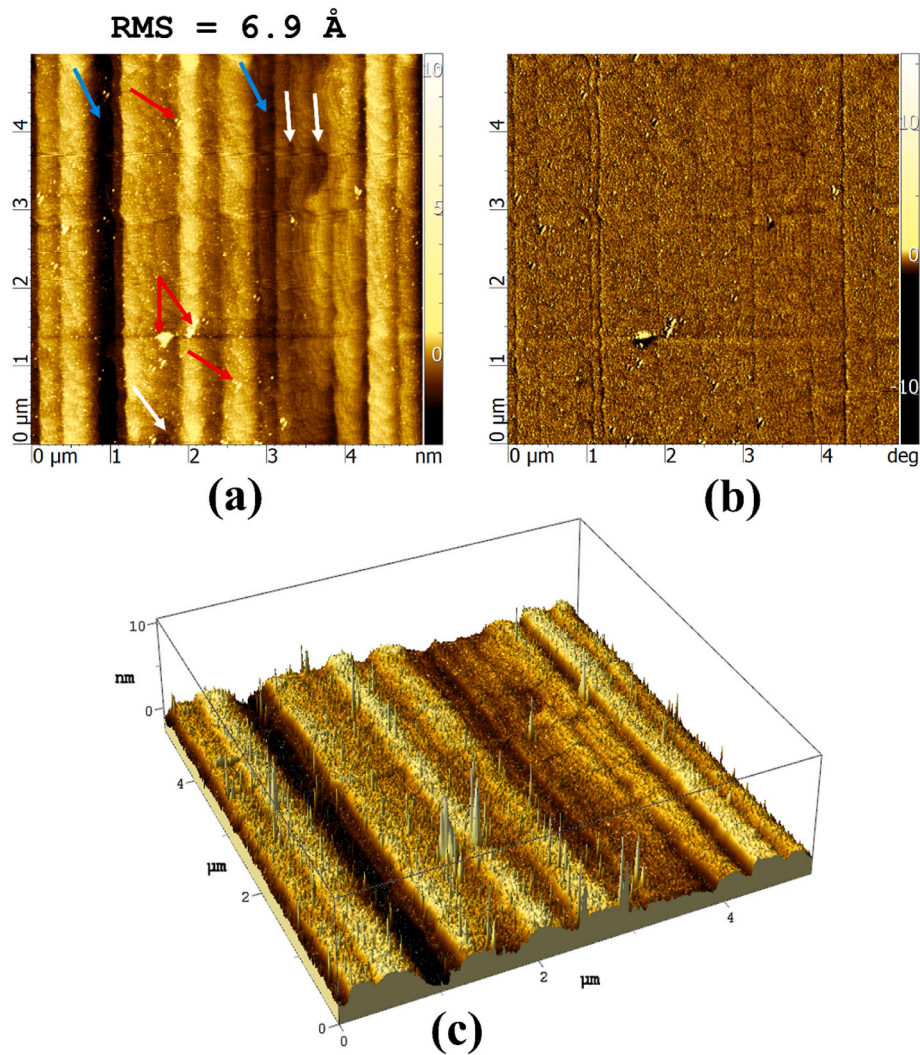


Fig. 12. 2D AFM (a) and (b) phase contrast micrographs and (c) 3D AFM micrograph with $5 \times 5 \mu\text{m}^2$ scan size of (100) oriented InGaAs/InP (Regarding the significance of arrows in (a): white arrows indicate pits, blue arrows show deeper and aligned pits along the surface, and red arrows show 3D-islands where the combined one points the mega-islands).

fitted by the semi-empirical models and modified semi-empirical models based on the LSE model. This latter indicates an anomalous behavior in the LT range giving an S-shape form deviated from the conventional behavior announced by the semi-empirical Viña and Pässler models: energy is decreased with temperature due to the thermal agitation and the lattice expansion (in the high-temperature range). The LSE simulation is consistent well with the experimental points. It is worthy to note that all the fitting curves are superposed at higher temperatures. In both semi-empirical and LSE frames, the energy falls linearly with the PL data at high temperatures where the fitting parameters are summarized in Table 3.

As the empirical Varshni model fits the PL bandgap evolution at the Debye temperature $\theta_D = 346 \text{ K}$, the effective temperature $\mathcal{G}_{eff} = \frac{2}{3}\theta_D$ [64] will be 231 K which is comparable with that of Pässler model in the LSE frame. This can prove the appropriacy of this model to fit the PL bandgap shrinkage more than that of Viña [64], as Fig. 16 (b) exhibits. It is well to note the different values of the bandgap energy extracted from UV-vis (0.748 eV) absorbance and the PL emission energy (0.718 eV) at room temperature. This shift is known as “Stokes shift” between absorption and emission spectra.

Numerous research works have been published to understand this phenomenon in In-containing samples and based on them [51,60, 65–70] we explain our finding: because of the surface segregation of

Indium, In-rich zones are created so called clusters that can trap carriers and behave like localized states. The S-shaped feature in PL energy evolution emphasizes our expectation about the non-uniform distribution of Indium, proved by SEM-EDX graphs and supports the fact that clustering effect, seen in AFM micrographs which in turn induced by the composition fluctuation, results in potential fluctuation, the most responsible for the abnormal PL behavior (S-shape) observed at low temperatures. The down-up-down evolution at low temperatures reflects the carrier trapping by the localized states in the sample-thermal transfer between localized states (from deep to shallower levels)-thermal activation of electron interaction with phonons.

Since the S-shape stems from the carriers’ redistribution between localized states and localized-delocalized states in the LSE formalism, a comparative analysis between Viña and Pässler models is introduced by studying the evolution of “ $K_B T.A(T)$ ” dimensionless term. Fig. 17 shows the reduction in characteristic temperature $T^{loc/deloc}$ by 15 K with an energetic increase of 8.3 meV in terms of the thermal redistribution of carriers in InGaAs alloy when comparing Viña to Pässler model.

It must however be emphasized that carriers were localized below $T^{loc/deloc}$, and after that temperature both of localization and delocalization processes are competitive so that the blueshift is recorded. Increasing continuously the temperature makes the carriers almost (partially or totally) delocalized and enhances their interaction with

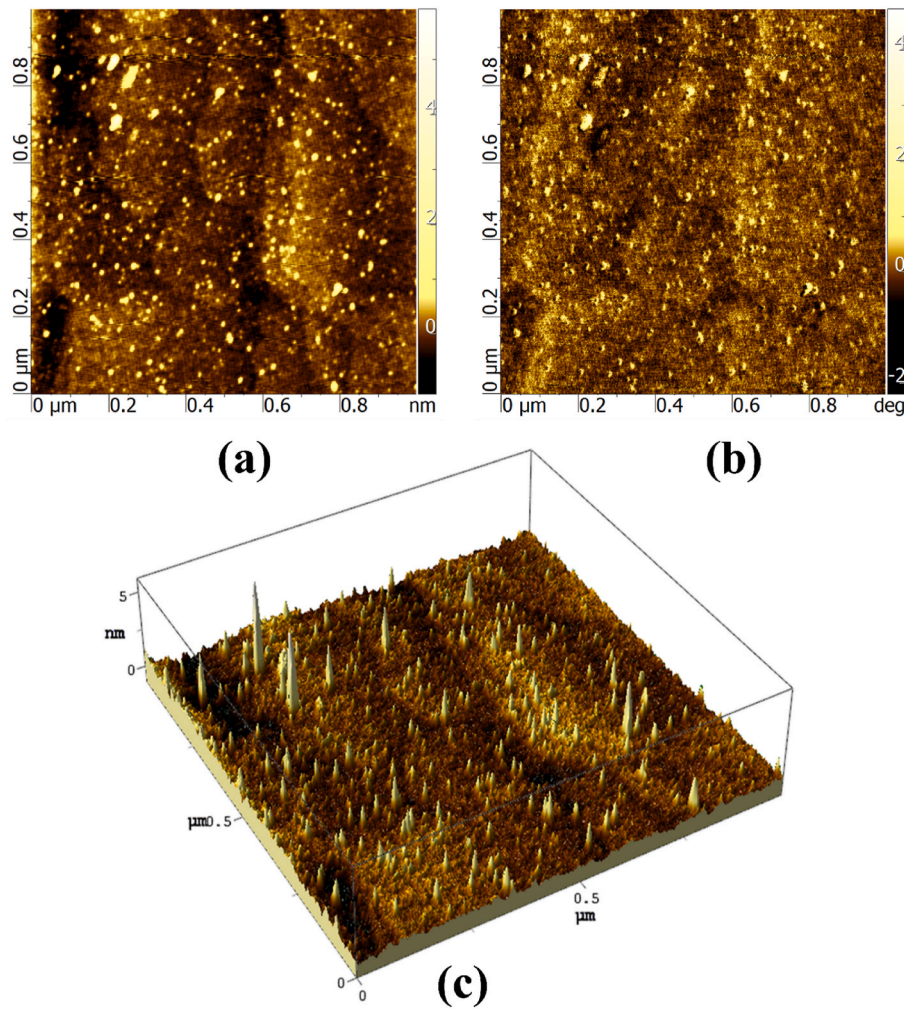


Fig. 13. 2D AFM (a) and (b) phase contrast micrographs and (c) 3D AFM micrograph with $1 \times 1 \mu\text{m}^2$ scan size of (100) oriented InGaAs/InP.

phonons leading to the bandgap energy shrinkage. In view of this, the thermal redistribution is higher in Viña approach than Pässler approach reflecting that the first redshift (band tail carriers will be re-trapped by deeper states) is overestimated by the modified Viña model: S-shape is not replicated very well in the low temperature range. The same for the contribution of delocalized carriers at higher temperatures: it is more significant for Viña model compared to Pässler model in the LSE frame where the delocalization of carriers is more rapid in the intermediate range, and it is comparable at high temperatures.

Carriers can be localized mainly because of the potential fluctuation due to clustering effects and/or the thickness fluctuation in quantum well (QW) and quantum dot (QD) heterostructures' interface [65]. As we made the growth of In-rich free buffer InGaAs layer on InP, we rule out the possible contribution of thickness fluctuation in such sample. Consequently, the potential fluctuation seems the only factor responsible for carrier localization due to the random and non-uniform distribution of Indium atoms within the structure, proved above by SEM-EDX and AFM micrographs.

The first redshift observed at the lowest temperatures indicates the re-localization of carriers by their redistribution i) between localized states (from shallow to deeper states) and/or from ii) delocalized to localized band tail energetic levels. Then, carriers start to delocalize at a specific temperature noted $T^{loc/deloc}$ where both localized and delocalized carriers contribute to the radiative recombination process. Further increase in temperature allows the total delocalization of carriers by thermally activating the phonon-electron interaction, resulting in the thermal bandgap energy shrinkage as the classic models stipulate.

This trend is highlighted in Fig. 16 (b) where all the fitting models are superposed at high temperatures. Regarding the illustrative schematic representation in Fig. 17, the delocalization process still incomplete where the dimensionless term $A(T) \cdot K_B T$, which reflects the re-trapping and thermal transfer of carriers, persists even for higher temperatures. Hidouri et al. have claimed that this result may be related to the lack of the numerical procedure [71].

To get in depth the thermal redistribution of carriers, we study in the following the spectral luminescence evolution in relation with the phonon's contribution.

The width of the InGaAs emission peak at half-maximum Γ depends on the temperature as described in Fig. 15, following equation (11) [72]

$$\Gamma(T) = \Gamma_0 + \Gamma_{LA} + \Gamma_{LO} + \Gamma_{imp} \tag{11}$$

Γ_0 is the temperature independent inhomogeneous width.

$\Gamma_{LA} = \eta_{LA} T$ designates the carrier interactions with acoustic phonons.

$\Gamma_{LO} = \frac{\eta_{LO}}{e^{\frac{E_{LO}}{K_B T}} - 1}$ presents Fröhlich interactions of carriers with optical phonons at elevated temperatures mainly in polar materials.

$\Gamma_{imp} = \frac{\eta_{imp}}{e^{\frac{E_{imp}}{K_B T}}}$ is linked to extrinsic mechanisms due to the non-idealities in the studied structure: alloy fluctuations, defect-related transitions, impurities, etc ...

As mentioned in Table 3, Pässler law follows the intermediate dispersion regime where the contribution of LA-phonon is more significant than that of LO-phonon. However, this model does not replicate

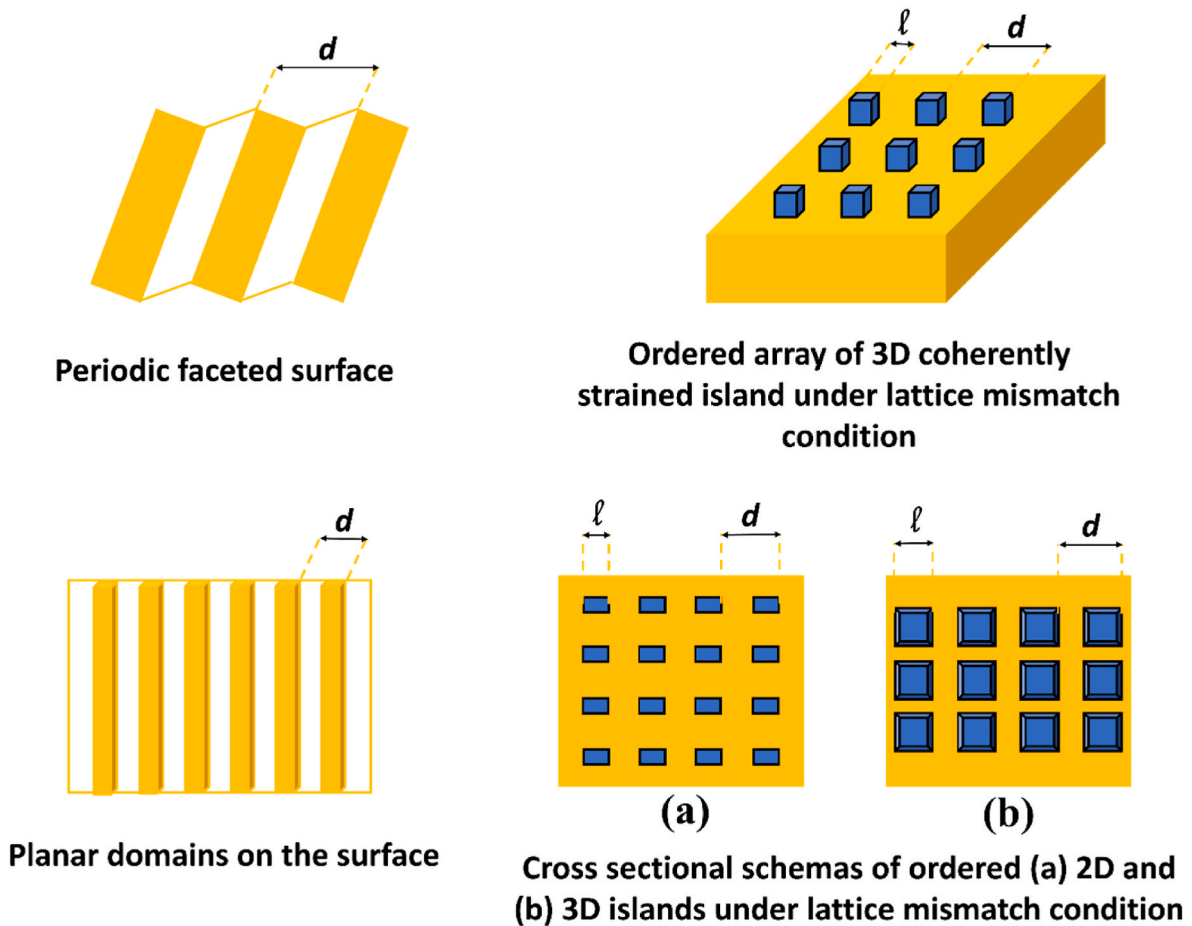


Fig. 14. Different classes of surface morphology in semi-conducting films.

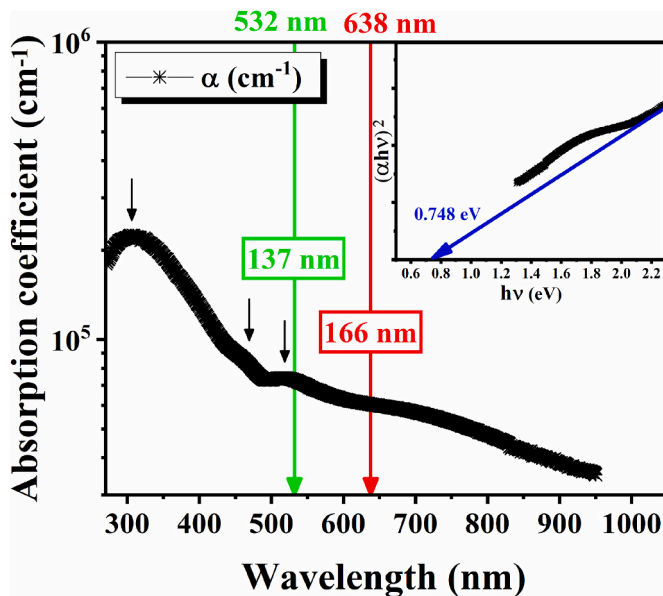


Fig. 15. UV-vis absorption measurement of InGaAs/InP (the inset illustrates the evolution of $(\alpha h\nu)^2$ versus $(h\nu)$ by identifying the bandgap energy of InGaAs $E_g^{RT} = 0.748 \text{ eV}$ at room temperature).

the S-shape feature. For that reason, we developed such a model in the LSE formalism showing another kind of phonon dispersion: a small dispersion regime where the LA-phonon contribution is negligible than

that of LO-phonon. Nevertheless, the contribution of both LO- and LA-phonon contributions still doubted when we analyze Fig. 18.

Γ_{imp} seems to be the only term that fits well the temperature dependency of the full width at half-maximum which reflects the high density of impurities in our system due to the alloy fluctuations (inhomogeneous distribution of Indium), proved by the SEM-EDX and AFM analysis, and the S-shaped form revealed by PL investigation. The large value of Γ_0 confirms the high density of non-idealities in such material justified by the inhomogeneous density of Indium atoms and the high induced residual strain [45] in the epitaxial layer, reported above. One can remark the fluctuation of the linewidth at the low temperature range [10–50] K, referred to the localized carriers, that continue to increase with temperature till $T_{sat} = 90 \text{ K}$ at which it stabilizes and restarts its rising at 150 K up to 300 K because of the activation of delocalized states at high temperatures and the phonon-assisted thermal contribution. In fact, the N-shape dependence is widely known as a fingerprint of carrier localization distinguishable from the exponential evolution of temperature dependent linewidth [73] and which is slightly shaped in our sample. At higher temperatures, the phonon assisted thermal transport will dominate the photoluminescence of InGaAs material. Thereby, the width of its spectrum will be larger and larger as indicated in Fig. 18 due to the frequent interaction of carriers with phonons. It is noteworthy that the high concentration of Indium and its non-uniform distribution within the structure, giving rise to high density of defects (translated by the large FWHM of PL spectra), surface roughness (shown in AFM micrographs) and dislocations will be detrimental for SWIR detection since such defect's density and heterointerface-induced strain led to higher dark current density, thereby poor SWIR detection [70,74].

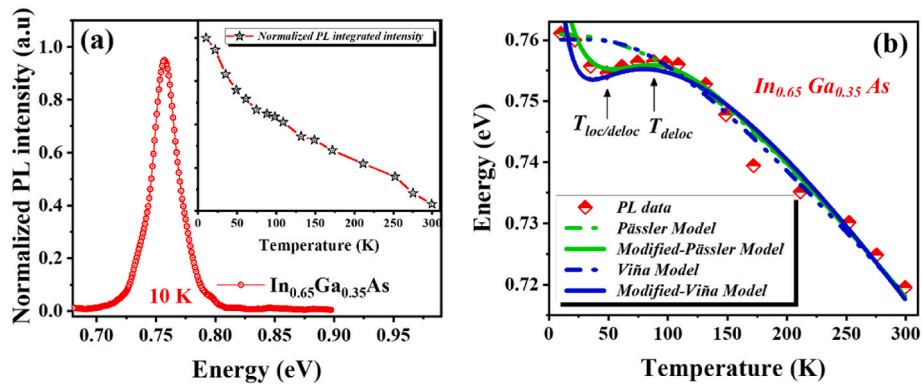


Fig. 16. (a) Low temperature photoluminescence LT PL-spectrum of InGaAs (inset: temperature dependent integrated PL intensity), (b) Temperature dependent photoluminescence TDPL energy fitted by semi-empirical and modified semi-empirical models.

Table 3
Optical fitting parameters used in semi-empirical and LSE configurations.

Models	Pässler	Modified Pässler (LSE frame)	Viña	Modified Viña (LSE frame)
E_0 (meV)	760	792.10	759.80	799.94
α ($\times 10^{-4}$ eV/K)	3.44	2.60	2.26 ^a	2.05 ^a
$\Theta_{i-B,P}(K)$	172	225	267	292
c	2.13	9	-	-
a_B (meV)	-	-	30.20	30
E_B (meV)	-	-	790	829.94
$T^{loc/deloc}(K)$	-	50	-	35
σ (meV)	-	5	-	3.70
$E_a - E_0$ (meV)	-	17.90	-	20.28

$$^a \alpha_{Viña} = \frac{2a_B}{\Theta_B} [63].$$

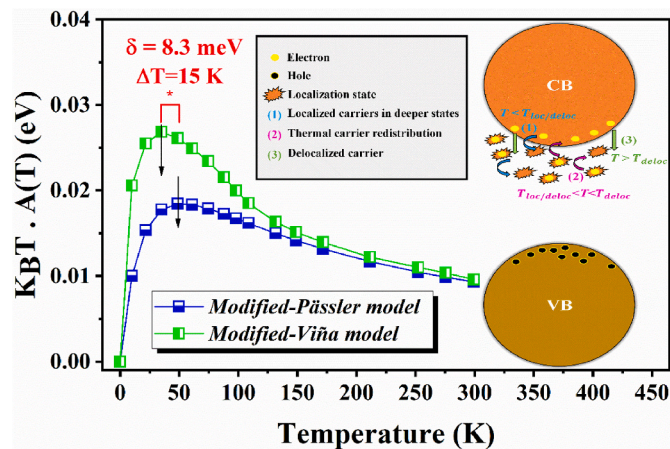


Fig. 17. Thermal redistribution of carriers over localized/delocalized states within $In_{0.65}Ga_{0.35}As$ structure using modified-Pässler and -Viña models in the LSE frame accompanied with illustrative schematic of the carriers' redistribution at the energy scale.

4. Conclusion

We carried out comprehensive studies of the crystallinity, composition, lattice vibrations, and optical characteristics of free buffer InGaAs thin film, successfully grown on InP substrate at 560 °C by MOVPE, with high Indium concentration. On one hand, structural analysis was performed: the XRD characterization demonstrated the higher crystallinity of the heterostructure. Then, SEM-EDX analysis showed the non-uniform distribution of Indium within the sample. Furthermore, Raman

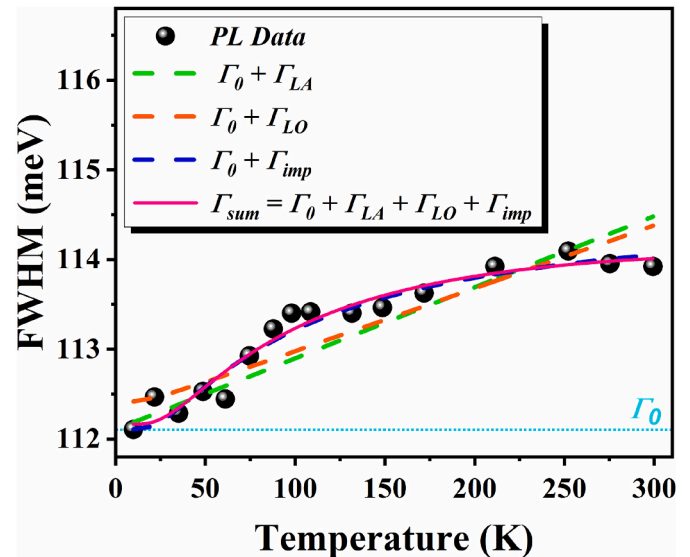


Fig. 18. Full width at half-maximum FWHM of the PL spectra plotted vs. temperature, with associated line width broadening fits.

scattering analysis allowed the identification of the presence of InAsP-like mode at 229.7 cm^{-1} . This finding was emphasized by the XRD shoulder of InP-related peak showing its compressive strain to InP layer. On an atomic scale, the AFM observation made it possible to study the surface morphology of our sample by showing its roughness and the proceeding growth mode in our epitaxy that was correlated with the optical response of InGaAs. The optical characterization was made to confirm the non-uniform distribution of Indium. Firstly, UV-vis measurement was performed to identify the absorption coefficient of InGaAs film and to estimate its bandgap energy at room temperature. Secondly, a temperature dependent photoluminescence characterization was carried out in the range 10–300 K to study the optical behavior of In-rich sample. The emission energy versus temperature revealed an S-shape feature due to the localization phenomenon. This reflected the potential fluctuation due to the composition fluctuation of Indium, proved by structural analysis. Moreover, the theoretical simulation reproduced the S-shaped form based on the semi-empirical models in the LSE frame, allowing to get in depth insight into physical concepts. The modified-Pässler model seemed to be the most accurate for reproducing the PL bandgap data, compared with the modified-Viña and the semi-empirical models, describing the thermal redistribution of carriers. Finally, the FWHM was also interpreted by considering the impurities, acoustic phonon and Fröhlich interactions with carriers in our semiconducting material where the contribution of impurities takes over the phonon

contribution (LO & LA modes). All these findings led to a concrete conclusion: In-rich structure can include composition fluctuation, impurities, and defects and may generate dislocations within the sample that can deteriorate its performance for SWIR application. In our future work, we will be investigating the same structure but with buffer layer to study its effect on the carrier localization by analyzing its structural and optical characteristics and their influence on the SWIR detection.

CRedit authorship contribution statement

Marwa Ben Arbia: Writing – review & editing, Writing – original draft, Visualization, Software, Formal analysis, Data curation, Conceptualization.

Declaration of competing interest

The authors declare that they have no known competing financial interests or personal relationships that could have appeared to influence the work reported in this paper.

Data availability

No data was used for the research described in the article.

References

- [1] C. Kwan, B. Chou, J. Yang, A. Rangamani, T. Tran, J. Zhang, R. Etienne-Cummings, Target tracking and classification using compressive measurements of MWIR and LWIR coded aperture cameras, *J. Signal Inf. Process.* 10 (2019) 73–95, <https://doi.org/10.4236/jsip.2019.103006>.
- [2] J.B. Kwon, S.W. Kim, B.H. Kang, S.H. Yeom, W.H. Lee, D.H. Kwon, J.S. Lee, S. W. Kang, Air-stable and ultrasensitive solution-cast SWIR photodetectors utilizing modified core/shell colloidal quantum dots, *Nano convergence* 7 (1) (2020) 1–10, <https://doi.org/10.1186/s40580-020-00238-3>.
- [3] M. Sulaman, S. Yang, T. Song, H. Wang, Y. Wang, H. Bo, D. Miao, Y. Tang, Y. Song, B. Zou, High performance solution-processed infrared photodiode based on ternary PbSxSe1-x colloidal quantum dots, *RSC Adv.* 6 (90) (2016) 87730–87737, <https://doi.org/10.1039/C6RA19946A>.
- [4] J. Liu, J. Lu, C. Yue, X. Li, H. Chen, L. Wang, InAs/InGaAs/InAlAs interband quantum well infrared photodetector (IQWIP) with cut-off response wavelength at 1.93 μm , *APEX Lett.* 3 (2019), 032005, <https://doi.org/10.7567/1882-0786/ab017f>.
- [5] H.W. Yoon, M.C. Dopkiss, G.P. Eppeldauer, Performance comparisons of InGaAs, extended InGaAs, and short-wave HgCdTe detectors between 1 μm and 2.5 μm , in: *Infrared Spaceborne Remote Sensing XIV*, vol. 6297, International Society for Optics and Photonics, 2006, September, p. 629703.
- [6] A. Tada, N. Namekata, S. Inoue, Saturated detection efficiency of single-photon detector based on an InGaAs/InP single-photon avalanche diode gated with a large-amplitude sinusoidal voltage, *Jpn. J. Appl. Phys.* 59 (7) (2020), 072004.
- [7] G.C. Jiao, X.B. Xu, L.D. Zhang, S.F. Wang, C.X. Peng, W. Cheng, C.L. Hu, Y.J. Zhou, C. Feng, InGaAs/InP photocathode grown by solid-source MBE, in: *International Symposium on Photoelectronic Detection and Imaging 2013: Low-Light-Level Technology and Applications*, vol. 8912, International Society for Optics and Photonics, 2013, August, 891216.
- [8] P. Gutowski, I. Sankowska, P. Karbownik, D. Pierścińska, O. Serebrennikova, M. Morawiec, E. Pruszyńska-Karbownik, K. Gołaszewska-Malec, K. Pierściński, J. Muszalski, M. Bugajski, MBE growth of strain-compensated InGaAs/InAlAs/InP quantum cascade lasers, *J. Cryst. Growth* 466 (2017) 22–29, <https://doi.org/10.1016/j.jcrysgro.2017.02.031>.
- [9] M. Udhayasankar, J. Kumar, P. Ramasamy, Growth and characterisation of InGaAs (P) by CBE technique, *J. Optoelectron. Adv. Mater.* 5 (1) (2003) 75–88.
- [10] L. Jiang, T. Lin, X. Wei, G.H. Wang, G.Z. Zhang, H.B. Zhang, X.Y. Ma, Effects of V/III ratio on InGaAs and InP grown at low temperature by LP-MOCVD, *J. Cryst. Growth* 260 (1–2) (2004) 23–27, <https://doi.org/10.1016/j.jcrysgro.2003.08.013>.
- [11] X. Li, J. Xu, T. Wei, W. Yang, S. Jin, Y. Wu, S. Lu, Enhanced properties of extended wavelength InGaAs on compositionally undulating step-graded InAsP buffers grown by molecular beam epitaxy, *Crystals* 11 (12) (2021) 1590, <https://doi.org/10.3390/cryst11121590>.
- [12] M.K. Hudait, Y. Lin, M.N. Palmisiano, C. Tivarus, J.P. Pelz, S.A. Ringel, Comparison of mixed anion, InAs y P 1-y and mixed cation, in x Al 1-x as metamorphic buffers grown by molecular beam epitaxy on (100) InP substrates, *J. Appl. Phys.* 95 (8) (2004) 3952–3960, <https://doi.org/10.1063/1.1667006>.
- [13] J. Guo, J. Zhao, M. Yang, Interface engineering of InGaAs/InP layer for photocathode, *Optik* 212 (2020), 164738.
- [14] L. Zhao, Z. Guo, M. Zhang, S. Yang, L. Zhao, Surface-interface analysis of InxGa1-xAs/InP heterostructure in positive and negative mismatch system, *Surf. Interface Anal.* 51 (5) (2019) 498–505, <https://doi.org/10.1002/sia.6609>.
- [15] M. Choi, I.Y. Jung, S. Song, C.S. Kim, Quantitative depth profile analysis of InP/InGaAs hetero-interfaces by as carry-over, *Mater. Sci. Semicond. Process.* 120 (2020), 105251, <https://doi.org/10.1016/j.mssp.2020.105251>.
- [16] S. Hernandez, N. Blanco, I. Martil, G. González-Díaz, R. Cuscó, L. Artus, Evidence of phosphorus incorporation into InGaAs/InP epilayers after thermal annealing, *J. Appl. Phys.* 93 (11) (2003) 9019–9023, <https://doi.org/10.1063/1.1565175>.
- [17] J. Decobert, G. Patriarche, Transmission electron microscopy study of the InP/InGaAs and InGaAs/InP heterointerfaces grown by metalorganic vapor-phase epitaxy, *J. Appl. Phys.* 92 (10) (2002) 5749–5755, <https://doi.org/10.1063/1.1513891>.
- [18] X.S. Jiang, A.R. Clawson, P.K.L. Yu, Study of interrupted MOVPE growth of InGaAs/InP superlattice, *J. Cryst. Growth* 124 (1–4) (1992) 547–552, [https://doi.org/10.1016/0022-0248\(92\)90515-K](https://doi.org/10.1016/0022-0248(92)90515-K).
- [19] S.W. Ryu, W.G. Jeong, I. Kim, H.D. Kim, H.H. Kim, B.D. Choe, S.H. Park, Reduction of as carryover by PH3 overpressure in metalorganic vapor-phase epitaxy, *J. Cryst. Growth* 179 (1–2) (1997) 26–31, [https://doi.org/10.1016/S0022-0248\(97\)00096-1](https://doi.org/10.1016/S0022-0248(97)00096-1).
- [20] H. Asahi, T. Kohara, R.K. Soni, K. Asami, S. Emura, S.I. Gonda, Atomically controlled InGaAs/InP superlattices grown by gas source MEE (migration enhanced epitaxy), *J. Cryst. Growth* 127 (1–4) (1993) 194–198, [https://doi.org/10.1016/0022-0248\(93\)90603-T](https://doi.org/10.1016/0022-0248(93)90603-T).
- [21] A.R. Clawson, T.T. Vu, S.A. Pappert, C.M. Hanson, Effects of hydrogen-only interrupts on InGaAs/InP superlattices grown by OMVPE, *J. Cryst. Growth* 124 (1–4) (1992) 536–540, [https://doi.org/10.1016/0022-0248\(92\)90513-1](https://doi.org/10.1016/0022-0248(92)90513-1).
- [22] T. Mozume, H. Kashima, K. Hosomi, K. Ouchi, H. Sato, H. Masuda, T. Tanoue, Effect of source-supply interruptions on the interface abruptness in gas source molecular beam epitaxy grown InGaAs/InP heterostructures, *J. Cryst. Growth* 150 (1995) 591–596, [https://doi.org/10.1016/0022-0248\(95\)80278-K](https://doi.org/10.1016/0022-0248(95)80278-K).
- [23] T. Mozume, H. Kashima, K. Hosomi, K. Ogata, K. Suenaga, A. Nakano, Tailored heterointerface formation in InGaAs/InP superlattices by gas source migration-enhanced epitaxy, *Appl. Surf. Sci.* 75 (1–4) (1994) 233–241, [https://doi.org/10.1016/0169-4332\(94\)90164-3](https://doi.org/10.1016/0169-4332(94)90164-3).
- [24] J.M. Vandenberg, S.N.G. Chu, Interface structure of large-period lattice matched InGaAs/InP superlattice grown by MOMB: a high-resolution X-ray diffraction study, *J. Cryst. Growth* 144 (1994) 9–12, [https://doi.org/10.1016/0022-0248\(94\)90003-5](https://doi.org/10.1016/0022-0248(94)90003-5).
- [25] B. Lakshmi, B.J. Robinson, D.T. Cassidy, D.A. Thompson, Anisotropic interfacial strain in InP/InGaAs/InP quantum wells studied using degree of polarization of photoluminescence, *J. Appl. Phys.* 81 (8) (1997) 3616–3620, <https://doi.org/10.1063/1.365479>.
- [26] M.J. Yates, M.R. Aylett, S.D. Perrin, P.C. Spurdens, Characterization of InP to GaInAs and GaInAs to InP interfaces using tilted cleaved corner TEM, *J. Cryst. Growth* 124 (1–4) (1992) 604–609, [https://doi.org/10.1016/0022-0248\(92\)90524-M](https://doi.org/10.1016/0022-0248(92)90524-M).
- [27] T. Anan, S. Sugou, K. Nishi, T. Ichihashi, Improvement of InP/InGaAs heterointerfaces grown by gas source molecular beam epitaxy, *Appl. Phys. Lett.* 63 (8) (1993) 1047–1049, <https://doi.org/10.1063/1.110765>.
- [28] A.Y. Lew, C.H. Yan, R.B. Welstand, J.T. Zhu, C.W. Tu, P.K.L. Yu, E.T. Yu, Interface structure in arsenide/phosphide heterostructure grown by gas-source MBE and low-pressure MOVPE, *J. Electron. Mater.* 26 (2) (1997) 64–69, <https://doi.org/10.1007/s11664-997-0089-5>.
- [29] J.M. Vandenberg, H. Temkin, R.A. Hamm, M.A. DiGiuseppe, Structural study of alloyed gold metallization contacts on InGaAs/InP layers, *J. Appl. Phys.* 53 (11) (1982) 7385–7389, <https://doi.org/10.1063/1.330364>.
- [30] B. Smiri, F. Saidi, A. Mlayah, H. Maaref, Comparative optical studies of InAlAs/InP quantum wells grown by MOCVD on (311) A and (311) B InP planes, *J. Mater. Sci. Mater. Electron.* 31 (2020) 10750–10759, <https://doi.org/10.1007/s10854-020-03625-y>.
- [31] K. Grodecki, K. Murawski, K. Michalczyk, B. Jankiewicz, P. Martyniuk, InAsSb mole fraction determination using Raman low energy modes, *Opt. Mater. Express* 10 (1) (2020) 149–154, <https://doi.org/10.1364/OME.10.000149>.
- [32] Z.C. Feng, A.A. Allerman, P.A. Barnes, S. Perkovitz, Raman scattering of InGaAs/InP grown by uniform radial flow epitaxy, *Appl. Phys. Lett.* 60 (15) (1992) 1848–1850, <https://doi.org/10.1063/1.107187>.
- [33] B. Smiri, F. Saidi, A. Mlayah, H. Maaref, Power- and temperature-dependent photoluminescence investigation of carrier localization at inverted interface transitions in InAlAs/InP structures, *Jpn. J. Appl. Phys.* 59 (2) (2020), <https://doi.org/10.7567/1347-4065/ab65a6>.
- [34] Z.V. Popović, A. Cantarero, J. Camacho, A. Milutinovi, O. Latinovi, L. González, Raman scattering and infrared reflectivity in [(In)P 5 (In 0.49 Ga 0.51 As) 8] 30 superlattices, *J. Appl. Phys.* 88 (11) (2000) 6382–6387, <https://doi.org/10.1063/1.1287133>.
- [35] Q.L. Wei, Z.X. Guo, L. Zhao, L. Zhao, D.Z. Yuan, G.Q. Miao, M.S. Xia, Structure optimization of high indium content InGaAs/InP heterostructure for the growth of in 0.82 Ga 0.18 as buffer layer, *Optoelectron. Lett.* 12 (6) (2016) 441–445, <https://doi.org/10.1007/s11801-016-6190-3>.
- [36] K. Radhakrishnan, T.H.K. Patrick, H.Q. Zheng, S.F. Yoon, Study of Raman Scattering on InP/InGaAs/InP HEMTs, vol. 588, MRS Online Proceedings Library (OPL), 1999, <https://doi.org/10.1557/PROC-588-167>.
- [37] A. Erol, E. Akalin, F. Sarcan, O. Donmez, S. Akycy, C.M. Arikian, J. Puustinen, M. Guina, Excitation energy-dependent nature of Raman scattering spectrum in GaInNAs/GaAs quantum well structures, *Nanoscale Res. Lett.* 7 (1) (2012) 1–8, <https://doi.org/10.1186/1556-276X-7-656>.
- [38] E. Poliani, M.R. Wagner, J.S. Reparaz, M. Mandl, M. Strassburg, X. Kong, A. Trampert, C.M. Sotomayor Torres, A. Hoffmann, J. Maultzsch, Nanoscale imaging of InN segregation and polymorphism in single vertically aligned InGaN/

- GaN multi quantum well nanorods by tip-enhanced Raman scattering, *Nano Lett.* 13 (7) (2013) 3205–3212, <https://doi.org/10.1021/nl401277y>.
- [39] M.S. Park, M. Razaee, K. Barnhart, C.L. Tan, H. Mohseni, Surface passivation and aging of InGaAs/InP heterojunction phototransistors, *J. Appl. Phys.* 121 (23) (2017), 233105, <https://doi.org/10.1063/1.4986633>.
- [40] A. Sayari, N. Yahyaoui, M. Ouelati, H. Maaref, K. Zellama, Raman study of V/III flux ratio effect in InP/InAlAs/InP heterostructures grown by MOCVD, *J. Raman Spectrosc.* 40 (8) (2009) 1023–1027, <https://doi.org/10.1002/jrs.2224>. International Journal for Original Work in all Aspects of Raman Spectroscopy, Including Higher Order Processes, and also Brillouin and Rayleigh Scattering.
- [41] J. Finders, M. Keuter, D. Gnoth, J. Geurts, J. Woitok, A. Kohl, R.R. Müller, K. Heime, Investigation of MOVPE-grown In_{0.53}Ga_{0.47}As/InP multi-quantum wells by Raman spectroscopy and X-ray diffractometry, in: European Materials Research Society Symposia Proceedings 40, 1993, January, pp. 161–164. <https://doi.org/10.1016/B978-0-444-81769-3.50014-0>.
- [42] J. Geurts, J. Finders, J. Woitok, D. Gnoth, A. Kohl, K. Heime, Characterization of the interface abruptness of In_{0.53}Ga_{0.47}As/InP multi quantum wells by Raman spectroscopy, X-ray diffractometry and photoluminescence, *J. Cryst. Growth* 145 (1–4) (1994) 813–818, [https://doi.org/10.1016/0022-0248\(94\)91147-9](https://doi.org/10.1016/0022-0248(94)91147-9).
- [43] S.R. Meher, A. Subrahmanyam, M.K. Jain, Composition-dependent structural, optical and electrical properties of x Ga_{1-x}N ($0.5 \leq x \leq 0.93$) thin films grown by modified activated reactive evaporation, *J. Mater. Sci.* 48 (3) (2013) 1196–1204, <https://doi.org/10.1007/s10853-012-6859-3>.
- [44] S. Emura, S.I. Gonda, Y. Matsui, H. Hayashi, Internal-stress effects on Raman spectra of x Ga_{1-x}As on InP, *Phys. Rev. B* 38 (5) (1988) 3280, <https://doi.org/10.1103/PhysRevB.38.3280>.
- [45] B. Smiri, M. Ben Arbia, D. Ilkay, F. Saidi, Z. Othmen, B. Dkhil, I. Altuntas, S. Elagoz, F. Hassen, H. Maaref, Optical and structural properties of In-rich In_xGa_{1-x}As epitaxial layers on (1 0 0) InP for SWIR detectors, *Mater. Sci. Eng., B* 262 (2020), 114769, <https://doi.org/10.1016/j.mseb.2020.114769>.
- [46] R. Bernal Correa, J. Montes Monsalve, A. Pulzara Mora, M. López López, A. Cruz Orea, J.A. Cardona, Polycrystalline growth of zinc blende gallium arsenide layers by RF magnetron sputtering, *Superficies y vacío* 27 (3) (2014) 102–106.
- [47] M. Kitamura, M. Nishioka, R. Schur, Y. Arakawa, Direct observation of the transition from a 2D layer to 3D islands at the initial stage of InGaAs growth on GaAs by AFM, *J. Cryst. Growth* 170 (1–4) (1997) 563–567.
- [48] N. Ohtani, M. Katsuno, T. Aigo, T. Fujimoto, H. Tsuge, H. Yashiro, M. Kanaya, Step bunching behaviour on the {0 0 1} surface of hexagonal SiC, *J. Cryst. Growth* 210 (4) (2000) 613–622, [https://doi.org/10.1016/S0022-0248\(99\)00877-5](https://doi.org/10.1016/S0022-0248(99)00877-5).
- [49] T. Kikkawa, K. Makiyama, H. Ochimizu, K. Kasai, J. Komeno, Effect of strained InGaAs step bunching on mobility and device performance in n-InGaP/InGaAs/GaAs pseudomorphic heterostructures grown by metalorganic vapor phase epitaxy, *J. Cryst. Growth* 145 (1–4) (1994) 799–807.
- [50] P. Tejedor, M. Drescher, L. Vázquez, L. Wilde, Epitaxial n++-InGaAs ultra-shallow junctions for highly scaled n-MOS devices, *Appl. Surf. Sci.* 496 (2019), 143721, <https://doi.org/10.1016/j.apsusc.2019.143721>.
- [51] L. Gu, J. Meng, The influence of growth parameters of strain InGaAs quantum wells on luminescent properties, *J. Electron. Mater.* 51 (3) (2022) 1421–1427, <https://doi.org/10.1007/s11664-021-09394-6>.
- [52] S. Kang, J. Kim, C.W. Jang, H. Jang, S.T. Lee, B.H. Lee, S. Kim, C.S. Shin, D.H. Jun, Thermally induced metastability of InGaAs single-layer for highly strained superlattices by metal-organic chemical vapor deposition, *J. Alloys Compd.* 905 (2022), 164252, <https://doi.org/10.1016/j.jallcom.2022.164252>.
- [53] K. Bellmann, U.W. Pohl, C. Kuhn, T. Wernicke, M. Kneissl, Controlling the morphology transition between step-flow growth and step-bunching growth, *J. Cryst. Growth* 478 (2017) 187–192, <https://doi.org/10.1016/j.jcrysgro.2017.09.007>.
- [54] D.J. Srolovitz, On the stability of surfaces of stressed solids, *Acta Metall.* 37 (2) (1989) 621–625, [https://doi.org/10.1016/0001-6160\(89\)90246-0](https://doi.org/10.1016/0001-6160(89)90246-0).
- [55] D.E. Jesson, K.M. Chen, S.J. Pennycook, T. Thundat, R.J. Warmack, Morphological evolution of strained films by cooperative nucleation, *Phys. Rev. Lett.* 77 (7) (1996) 1330, <https://doi.org/10.1103/PhysRevLett.77.1330>.
- [56] A. Gocalinska, M. Manganaro, E. Pelucchi, Suppression of threading defects formation during Sb-assisted metamorphic buffer growth in InAs/InGaAs/InP structure, *Appl. Phys. Lett.* 100 (15) (2012), 152112, <https://doi.org/10.1063/1.3703587>.
- [57] M. Udhayasankar, J. Kumar, P. Ramasamy, Growth and characterisation of InGaAs (P) by CBE technique, *J. Optoelectron. Adv. Mater.* 5 (1) (2003) 75–88.
- [58] J. Mudron, J. Mullerova, F. Dubecky, J. Huran, Optical properties of semi-insulating InP: Fe irradiated by fast neutrons, in: ASDAM'98. Conference Proceedings. Second International Conference On Advanced Semiconductor Devices And Microsystems (Cat, IEEE, 1998, October, pp. 235–238, <https://doi.org/10.1109/ASDAM.1998.730207>. No. 98EX172).
- [59] V.K. Dixit, S. Porwal, S.D. Singh, T.K. Sharma, S. Ghosh, S.M. Oak, A versatile phenomenological model for the S-shaped temperature dependence of photoluminescence energy for an accurate determination of the exciton localization energy in bulk and quantum well structures, *J. Phys. Appl. Phys.* 47 (6) (2014), 065103, <https://doi.org/10.1088/0022-3727/47/6/065103>.
- [60] Q. Li, S.J. Xu, W.C. Cheng, M.H. Xie, S.Y. Tong, C.M. Che, H. Yang, Thermal redistribution of localized excitons and its effect on the luminescence band in InGaN ternary alloys, *Appl. Phys. Lett.* 79 (12) (2001) 1810–1812, <https://doi.org/10.1063/1.1403655>.
- [61] M. Bennour, L. Bouzaïene, F. Saidi, L. Sfaxi, H. Maaref, Abnormal temperature dependencies of photoluminescence and carrier transfer in InAs QDs and DWELL structures grown on GaAs (1 1 5) A emitting near 1.3 μm wavelength, *J. Lumin.* 148 (2014) 207–213, <https://doi.org/10.1016/j.jlumin.2013.12.031>.
- [62] T. Hidouri, F. Saidi, H. Maaref, P. Rodriguez, L. Auvray, Impact of photoluminescence temperature and growth parameter on the exciton localized in BxGa_{1-x}As/GaAs epilayers grown by MOCVD, *Opt. Mater.* 60 (2016) 487–494, <https://doi.org/10.1016/j.optmat.2016.08.029>.
- [63] S.A. Lourenço, I.F.L. Dias, J.L. Duarte, E. Laureto, E.A. Meneses, J.R. Leite, I. Mazzaro, Temperature dependence of optical transitions in AlGaAs, *J. Appl. Phys.* 89 (11) (2001) 6159–6164, <https://doi.org/10.1063/1.1367875>.
- [64] B.K. Sarkar, A.S. Verma, P.S. Deviprasad, Temperature induced band gap shrinkage in Cu₂GeSe₃: role of electron-phonon interaction, *Phys. B Condens. Matter* 406 (14) (2011) 2847–2850, <https://doi.org/10.1016/j.physb.2011.04.045>.
- [65] S. Hammersley, D. Watson-Parris, P. Dawson, M.J. Godfrey, T.J. Badcock, M. J. Kappers, C. McAleese, R.A. Oliver, C.J. Humphreys, The consequences of high injected carrier densities on carrier localization and efficiency droop in InGaN/GaN quantum well structures, *J. Appl. Phys.* 111 (8) (2012), 083512, <https://doi.org/10.1063/1.3703062>.
- [66] Q. Li, S.J. Xu, M.H. Xie, S.Y. Tong, A model for steady-state luminescence of localized-state ensemble, *Europhys. Lett.* 71 (6) (2015) 994–1000, <https://doi.org/10.1209/epl/i2005-10170-7>.
- [67] I. Fraj, T. Hidouri, F. Saidi, H. Maaref, Carrier localization in In_{0.21}Ga_{0.79}As/GaAs multiple quantum wells: a modified Pässler model for the S-shaped temperature dependence of photoluminescence energy, *Superlattice. Microst.* 102 (2017) 351–358, <https://doi.org/10.1016/j.spmi.2016.12.051>.
- [68] I. Fraj, T. Hidouri, F. Saidi, L. Bouzaïene, L. Sfaxi, H. Maaref, Effect of carriers localization in clusters on optical properties of In_{0.21}Ga_{0.79}As/GaAs multiple quantum wells, *Curr. Appl. Phys.* 17 (2017) 1–5, <https://doi.org/10.1016/j.cap.2016.10.013>.
- [69] W. Liu, D.G. Zhao, D.S. Jiang, P. Chen, Z.S. Liu, J.J. Zhu, X. Li, F. Liang, J.P. Liu, S. M. Zhang, H. Yang, Y.T. Zhang, G.T. Du, The difference in efficiency droop behaviors of two InGaN/GaN multiple-quantum-well green light-emitting diodes with modified structural parameters, *Superlattice. Microst.* 88 (2015) 50–55, <https://doi.org/10.1016/j.spmi.2015.08.026>.
- [70] M. Ben Arbia, B. Smiri, I. Demir, F. Saidi, I. Altuntas, F. Hassen, H. Maaref, Theoretical analyses of the carrier localization effect on the photoluminescence of In-rich InGaAs layer grown on InP, *Mater. Sci. Semicond. Process.* 140 (2022), 106411, <https://doi.org/10.1016/j.mssp.2021.106411>.
- [71] T. Hidouri, R. Hamila, I. Fraj, F. Saidi, H. Maaref, P. Rodriguez, L. Auvray, Investigation of the localization phenomenon in quaternary BInGaAs/GaAs for optoelectronic applications, *Superlattice. Microst.* 103 (2017) 386–394, <https://doi.org/10.1016/j.spmi.2016.10.021>.
- [72] H. Esmailpour, V.R. Whiteside, L.C. Hirst, J.G. Tischler, C.T. Ellis, M.P. Lumb, D. V. Forbes, R.J. Walters, I.R. Sellers, Effect of occupation of the excited states and phonon broadening on the determination of the hot carrier temperature from continuous wave photoluminescence in InGaAsP quantum well absorbers, *Progress in Photovoltaics: Res. Appl.* 25 (9) (2017) 782–790, <https://doi.org/10.1002/pip.2890>.
- [73] F.-I. Laia, S.Y. Kuo, J.S. Wang, R.S. Hsiao, H.C. Kuo, J. Chic, S.C. Wang, H.S. Wang, C.T. Liang, Y.F. Chen, Temperature-dependent optical properties of In_{0.34}Ga_{0.66}As_{1-x}N_x single quantum well with high nitrogen content for 1.55 μm application grown by molecular beam epitaxy, *J. Cryst. Growth* 291 (1) (2006) 27–33, <https://doi.org/10.1016/j.jcrysgro.2006.02.028>.
- [74] X. Ji, B. Liu, H. Tang, X. Yang, X. Li, H. Gong, B. Shen, P. Han, F. Yan, 2.6 μm MBE grown InGaAs detectors with dark current of SRH and TAT, *AIP Adv.* 4 (8) (2014), 087135, <https://doi.org/10.1063/1.4894142>.

The power of the Web of Science™ on your mobile device, wherever inspiration strikes.

Dismiss

Learn More

Already have a manuscript?

Use our Manuscript Matcher to find the best relevant journals!

Find a Match

Filters

Clear All

Web of Science Coverage 

Open Access  

Category 

Country / Region 

Language 

Frequency 

Journal Citation Reports 

Refine Your Search Results

Materials Science in Semiconductor Processing

Search

Sort By: Relevancy 

Search Results

Found 21,865 results (Page 1)

[Share These Results](#)

Exact Match Found

MATERIALS SCIENCE IN SEMICONDUCTOR PROCESSING

Publisher: ELSEVIER SCI LTD , 125 London Wall, London, England, EC2Y 5AS

ISSN / eISSN: 1369-8001 / 1873-4081

Web of Science Core Collection: Science Citation Index Expanded

Additional Web of Science Indexes: Current Contents Electronics & Telecommunications Collection | Current Contents Engineering, Computing & Technology | Current Contents Physical, Chemical & Earth Sciences | Essential Science Indicators

[Share This Journal](#)

[View profile page](#)

* Requires free login.

Other Possible Matches

APPLIED PHYSICS A-MATERIALS SCIENCE & PROCESSING

Publisher: SPRINGER HEIDELBERG , TIERGARTENSTRASSE 17, HEIDELBERG, GERMANY, D-69121

ISSN / eISSN: 0947-8396 / 1432-0630

Web of Science Core Collection: Science Citation Index Expanded

Additional Web of Science Indexes: Current Contents Electronics & Telecommunications Collection | Current Contents Physical, Chemical & Earth Sciences | Essential Science Indicators

[Share This Journal](#)

[View profile page](#)

* Requires free login.



MATERIALS SCIENCE AND ENGINEERING A-STRUCTURAL MATERIALS PROPERTIES MICROSTRUCTURE AND PROCESSING

Publisher: **ELSEVIER SCIENCE SA , PO BOX 564, LAUSANNE, SWITZERLAND, 1001**

ISSN / eISSN: **0921-5093 / 1873-4936**

Web of Science Core Collection: **Science Citation Index Expanded**

Additional *Web of Science* Indexes: **Current Contents Engineering, Computing & Technology | Current Contents Physical, Chemical & Earth Sciences | Essential Science Indicators**

[Share This Journal](#)

[View profile page](#)

** Requires free login.*

METALLURGICAL AND MATERIALS TRANSACTIONS B-PROCESS METALLURGY AND MATERIALS PROCESSING SCIENCE

Publisher: **SPRINGER , ONE NEW YORK PLAZA, SUITE 4600 , NEW YORK, United States, NY, 10004**

ISSN / eISSN: **1073-5615 / 1543-1916**

Web of Science Core Collection: **Science Citation Index Expanded**

Additional *Web of Science* Indexes: **Current Contents Engineering, Computing & Technology | Essential Science Indicators**

[Share This Journal](#)

[View profile page](#)

** Requires free login.*

CURRENT OPINION IN SOLID STATE & MATERIALS SCIENCE

Publisher: **PERGAMON-ELSEVIER SCIENCE LTD , THE BOULEVARD, LANGFORD LANE, KIDLINGTON, OXFORD, ENGLAND, OX5 1GB**

ISSN / eISSN: **1359-0286 / 1879-0348**

Web of Science Core Collection: **Science Citation Index Expanded**

Additional *Web of Science* Indexes: **Current Contents Electronics & Telecommunications Collection | Current Contents Engineering, Computing & Technology | Current Contents Physical, Chemical & Earth Sciences | Essential Science Indicators**

[Share This Journal](#)

[View profile page](#)

** Requires free login.*

JOURNAL OF MATERIALS SCIENCE

Publisher: **SPRINGER , ONE NEW YORK PLAZA, SUITE 4600 , NEW YORK, United States, NY, 10004**

ISSN / eISSN: **0022-2461 / 1573-4803**

Web of Science Core Collection: **Science Citation Index Expanded**

Additional *Web of Science* Indexes: **Current Contents Electronics & Telecommunications Collection | Current Contents Engineering, Computing & Technology | Current Contents Physical, Chemical & Earth Sciences | Essential Science Indicators**



Science
Indexes:

[Share This Journal](#)

[View profile page](#)

* Requires free login.

JOURNAL OF MATERIALS SCIENCE-MATERIALS IN ELECTRONICS

Publisher: **SPRINGER , VAN GODEWIJCKSTRAAT 30, DORDRECHT, NETHERLANDS, 3311 GZ**

ISSN / eISSN: **0957-4522 / 1573-482X**

Web of Science Core Collection: **Science Citation Index Expanded**

Additional *Web of Science* Indexes: **Current Contents Electronics & Telecommunications Collection | Current Contents Engineering, Computing & Technology | Current Contents Physical, Chemical & Earth Sciences | Essential Science Indicators**

[Share This Journal](#)

[View profile page](#)

* Requires free login.

JOURNAL OF MATERIALS SCIENCE & TECHNOLOGY

Publisher: **JOURNAL MATER SCI TECHNOL , 72 WENHUA RD, SHENYANG, PEOPLES R CHINA, 110015**

ISSN / eISSN: **1005-0302 / 1941-1162**

Web of Science Core Collection: **Science Citation Index Expanded**

Additional *Web of Science* Indexes: **Current Contents Electronics & Telecommunications Collection | Current Contents Engineering, Computing & Technology | Essential Science Indicators**

[Share This Journal](#)

[View profile page](#)

* Requires free login.

JOURNAL OF SEMICONDUCTOR TECHNOLOGY AND SCIENCE

Publisher: **IEEK PUBLICATION CENTER , RM #907 SCIENCE & TECHNOLOGY NEW BLDG, 635-4 YUCKSAM-DONG, SEOUL, SOUTH KOREA, KANGNAM-KU, 135-703**

ISSN / eISSN: **1598-1657 / 2233-4866**

Web of Science Core Collection: **Science Citation Index Expanded**

Additional *Web of Science* Indexes: **Current Contents Electronics & Telecommunications Collection | Current Contents Engineering, Computing & Technology | Essential Science Indicators**

[Share This Journal](#)

[View profile page](#)

* Requires free login.



SEMICONDUCTOR SCIENCE AND TECHNOLOGY

Publisher: **IOP PUBLISHING LTD , TEMPLE CIRCUS, TEMPLE WAY, BRISTOL, ENGLAND, BS1 6BE**

ISSN / eISSN: **0268-1242 / 1361-6641**

Web of Science Core Collection: **Science Citation Index Expanded**

Additional *Web of Science* Indexes: **Current Contents Electronics & Telecommunications Collection | Current Contents Physical, Chemical & Earth Sciences | Essential Science Indicators**

[Share This Journal](#)

[View profile page](#)

* Requires free login.

Editorial Disclaimer: As an independent organization, Clarivate does not become involved in and is not responsible for the editorial management of any journal or the business practices of any publisher. Publishers are accountable for their journal performance and compliance with ethical publishing standards. The views and opinions expressed in any journal are those of the author(s) and do not necessarily reflect the views or opinions of Clarivate. Clarivate remains neutral in relation to territorial disputes, and allows journals, publishers, institutes and authors to specify their address and affiliation details including territory.

Criteria for selection of newly submitted titles and re-evaluation of existing titles in the Web of Science are determined by the Web of Science Editors in their sole discretion. If a publisher's editorial policy or business practices negatively impact the quality of a journal, or its role in the surrounding literature of the subject, the Web of Science Editors may decline to include the journal in any Clarivate product or service. The Web of Science Editors, in their sole discretion, may remove titles from coverage at any point if the titles fail to maintain our standard of quality, do not comply with ethical standards, or otherwise do not meet the criteria determined by the Web of Science Editors. If a journal is deselected or removed from coverage, the journal will cease to be indexed in the Web of Science from a date determined by the Web of Science Editors in their sole discretion – articles published after that date will not be indexed. The Web of Science Editors' decision on all matters relating to journal coverage will be final.

Clarivate.™ Accelerating innovation.

© 2023 Clarivate

[Legal center](#)

[Privacy notice](#)

[Cookie policy](#)

[Tanımlama Bilgisi Ayarları](#)

[Copyright notice](#)

[Help](#)

